SKB TECHNICAL REPORT

86-23

Settlement of Canisters with Smectite Clay envelopes in Deposition Holes

Roland Pusch
Swedish Geological Co

December 1986

SETTLEMENT OF CANISTERS WITH SMECTITE CLAY ENVELOPES IN
DEPOSITION HOLES

Roland Pusch
Swedish Geological Co, Lund

December 1986

SETTLEMENT OF CANISTERS WITH SMECTITE CLAY ENVELOPES IN DEPOSITION HOLES

Roland Pusch

Swedish Geological Co

December 1986

CONTENTS

SUMMARY

Settlement of canisters containing radioactive waste and being sur-
rounded by dense smectite clay is caused by the stresses and heat
induced in the clay. Consolidation by water expulsion of the clay
underlying a model canister with 5 cm diameter and 30 cm length
would theoretically account for a maximum finite settlement of about
70 μm in a few weeks, while shear-induced creep in the form of
viscous flow under constant volume conditions would yield a settle-
ment of only a few microns in the same time period according to a
previously developed theoretical model. These predictions were check-
ed by running a laboratory test in which a dead load of 80 kg was
applied to a small cylindrical copper canister embedded in Na bento-
nite with a density of 2.07 t/m^3.

The settlement, which increased in proportion to log time, turned out
to be about 6 μm in the first 2.5 months, which indicated that shear-
induced creep under constant volume conditions was the major settle-
ment-producing mechanism. This was confirmed at the end of the test
when sampling showed that no consolidation had taken place. After the
first loading period at room temperature, heating to 50°C and, after
a 4 months long "room temperature" period, to 70°C took place. This
cycling gave strong, instant settlement and upheaval because of the
different thermal expansion of the interacting components of the
system: the outer steel casing, the clay, and the canister. After the
development of constant temperature conditions in the entire system
and completion of the consolidation or expansion that followed from
the thermo-mechanical interactions, the settlement proceeded at a
rather high rate at 70°C, still following a log time creep law, but
with somewhat stronger retardation. At room temperature, i.e. in the
post-heating periods, the settlement seemed to cease, on the other
hand.

The conclusion from the study is that the canister movements under
isothermal conditions were in accordance with the log t-type creep
settlement that was predicted on theoretical grounds. Pre-heating and
low stresses may account for extraordinary retardation of the settle-
ment.

1   INTRODUCTION

The Swedish KBS 3 "multibarrier" concept for the disposal of highly radioactive, unreprocessed reactor fuel implies that 20-ton copper canisters containing such waste be surrounded by dense Na bentonite clay with montmorillonite as major constituent (Fig 1). Repositories consisting of arrays of tunnels with deposition holes drilled for canisters are planned to be located in crystalline rock at a minimum depth of 500 m. The tunnels will be backfilled with on-site compacted, relatively dense sand/bentonite mixtures, while the canister envelopes, which are expected to be almost impermeable for many thousand years, will consist of close-fitting blocks of heavily precompacted bentonite powder. A suitable raw material is commercial, air-dry Na bentonite granulate with a water content of 10-12 %. At compaction pressures of about 100 MPa the bulk density becomes about 2.1-2.2 t/m^3, and the degree of water saturation 50-60 %. After insertion in the deposition holes the blocks absorb water from the rock, swell and fill the initial small gap between the canisters and the confining rock. Hereby, the blocks get welded together so that the entire bentonite mass becomes virtually homogeneous with no visible joints, as demonstrated by long term field experiments (1).

As soon as the canisters come to rest on the underlying bentonite blocks, there will be a slight visco-elastic settlement of the yet not water saturated bentonite, but since this part of the clay envelope is expected to absorb water faster than the rest of the clay mass, the settlement soon stops and upheaval of the canister will instead take place. This movement will cease when the upper part of the mass has become largely wetted after which settlement will again take place.

The various movements that occur in the several years or even decades which pass before the water saturation is complete are developed in conjunction with initial homogenization processes and are of limited interest. The canister movement of major importance is naturally the long term settlement that takes place at elevated temperature in the first few thousand years and thereafter at normal rock temperature in 100.000 years or more. This secular settlement has been the subject of SKB-supported research in the last few years, the present report

summarizing current ideas concerning the involved physical processes and also the result of a precision model test in which the settlement of a model canister was measured for about 1.5 years.

The mechanisms which produce settlement have a very complex nature and depend very much on the physical state of the clay mineral montmorillonite with associated water, which is still not completely understood. Any discussion of the cause and character of the settlement needs to be based on the constitution of water-saturated montmorillonite, which is therefore briefly described in the introductory chapter.

BENTONITE/QUARTZ;
WEIGHT
RELATIONSHIP
1:10 TO 1:5

CANISTER

HIGHLY COMPACTED
BENTONITE

7.5 m

4.5

0.5

1.5
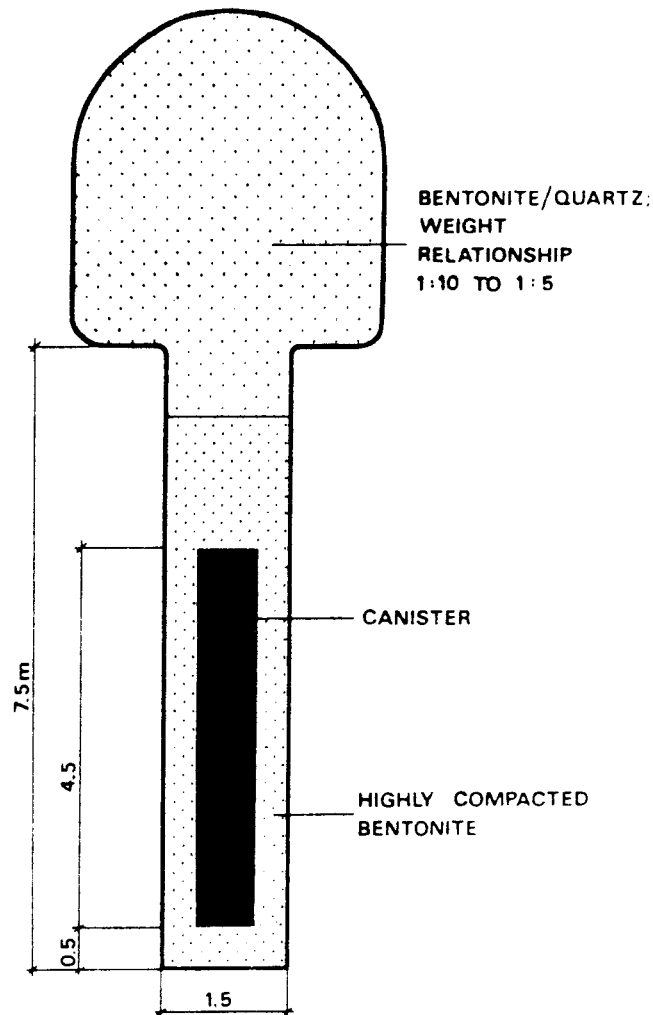
Fig 1. Cross section of tunnel at 500 m depth with clay-enveloped
        canister

2   CONSTITUTION OF WATER SATURATED MONTMORILLONITE CLAY

2.1   The mineral montmorillonite

There are two possible crystal lattice models for montmorillonite, i.e. the Hofmann/Endell/Wilm (HEW) version and the one suggested by Edelman and Favejee (EF). They cannot be distinguished on the basis of XRD or chemical analyses, and are represented by the compositions in Eqs (1) and (2) and the atomic arrangements shown in Fig 2. Both will be referred to in the subsequent text since it is presently not known which model actually applies and their atom lattice configurations are determinants of the physical state of a significant part of the porewater.

nH₂O   nH₂O

O O   ◎ OH   O Al   • Si
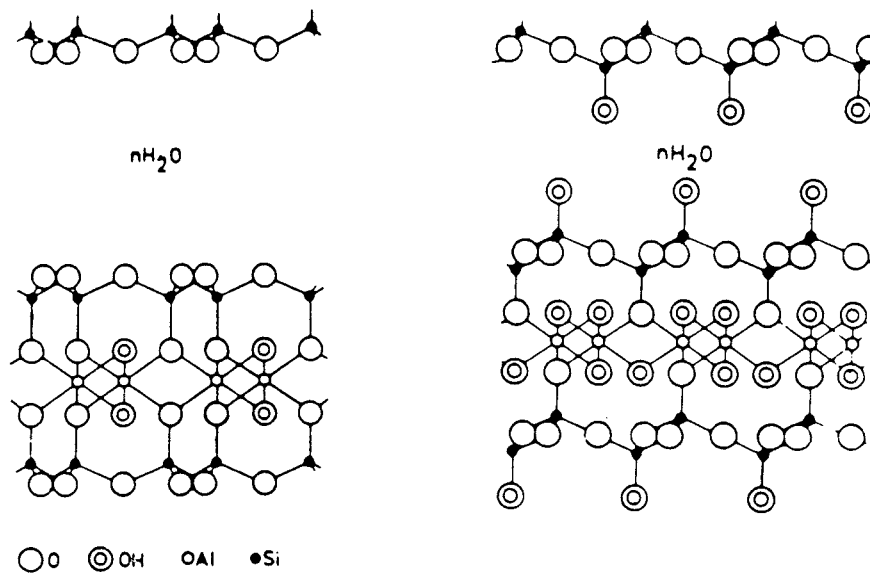
Fig 2.   The montmorillonite crystal lattice. Left: The HEW structure.
          Right: The EF structure

HEW: $(Si_8) (Al_{4-x} Mg_x) O_{20} (OH)_4 M^+$ (1)

EF: $(Si_8) (Al_{4-x} Mg_x) O_{16} (OH)_{12} M^+$ (2)
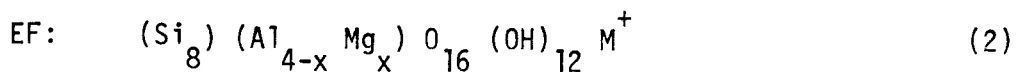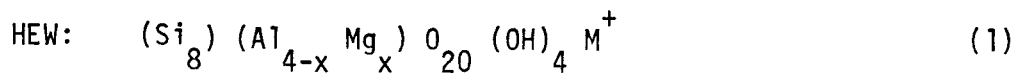
The EF model deviates from the traditionally favored HEW structure with respect to the type of coordination of the tetrahedra, termed trans - for the EF structure and cis - for the HEW version. We see

that every second tetrahedron of the silicious sheets is inverted, thus exposing apical OH:s which absorb water through hydrogen bonding and which can also exchange the proton (2, 3). Since only about 20 % of the cation exchange capacity appears to be due to such place exchange, the model has later been adjusted to one with a smaller number of inverted tetrahedrons although this correction may not be required (2, 4).

Various NMR studies have been conducted in order to identify which of the two crystal versions that is actually valid but there is no unanimous conclusion. However, one of the more comprehensive investigations suggests that both versions may be true, the EF model at temperatures exceeding 100°C and the HEW version at lower temperatures (2,5).

2.2 Montmorillonite/water interaction

The hydration of the Edelman & Favejee structure has been explained as the formation of an ice-like water lattice that grows from the protruding hydroxyls of the basal planes when the interlamellar cations are monovalent and small (Li and Na). A number of metastable and stable states of the H-bonded lattice may be established as shown in Fig 3, according to which the lattice does not spontaneously expand beyond 3 hydrate layers unless mechanical agitation causes separation of layers.

The wetting of the conventional Hofmann, Endell & Wilm structure is associated with the hydration of interlamellar cations. Water is first assumed to be distributed over external surfaces of stacks of lamellae ("domains") and then to yield successive hydration of the interlamellar space.

Like in the case of the EF model, interlamellar water lattices may be established on wetting of the Hofmann, Endell & Wilm structure but the spatial arrangement of the water molecules is largely determined by the position of interlamellar exchangeable cations, which in turn depends on the location of the deficit of positive clay lattice charge. The orientation and mutual interaction of the water molecules as well as their association with the interlamellar cations and the

crystal lattice are altered in the successive build-up of interlamel-
lar hydrates, the expected degree of ordering being low particularly
of the second and third hydrates. A model of the spatial arrangement
of the first layer of interlamellar water molecules in montmorillo-
nite containing monovalent exchangeable cations worked out by Sposito
(6) implies a strained ice-like configuration similar to Forslind's
lattice.
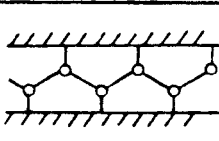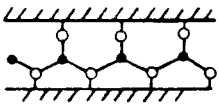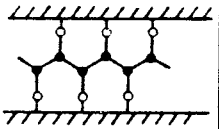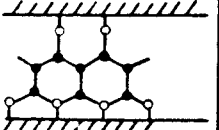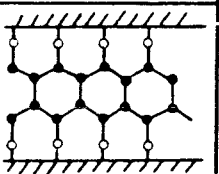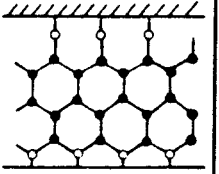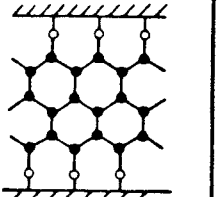
	SCHEMATIC INTER-LAYER STRUCTURE	H₂O MOLECULES PER UNIT CELL	BASAL SPACING Å	g H₂O/g CLAY	mM H₂O PER g CLAY	REMARKS
0		0	12.30	0 0.084 AT COMPLETE DEHYDROXYL ATION	0 4.667 AT COMPLETE DEHYDROXYL ATION	UNSTABLE NO HYDRATION : 4 OH-GROUPS PER UNIT CELL
1		2.66	15.05	0.059	3.278	UNSTABLE
2		5.33	17.81	0.119	6.661	STABLE MONOLAYER
3		8.0	18.73	0.179	9.944	UNSTABLE
4		10.67	21.49	0.238	13.222	STABLE 2 LAYERS
5		13.32	22.41	0.297	16.5	UNSTABLE
6		16.0	25.17	0.357	19.833	STABLE 3 LAYERS

Fig 3. Water lattice configuration in interlamellar positions of Li-
or Na montmorillonite (After Forslind)

2.3 Microstructure

2.3.1 Influence of hydration and homogenization

The water uptake and swelling of the confined clay blocks in deposition holes is associated with gradual improvement in microstructural homogeneity as indicated by Fig 4. This picture shows that the individual granules are characterized by a high degree of orientation of the montmorillonite lamellae that is inherited from the fabric of the natural bentonite beds, and that the granules are randomly oriented. The virgin as well as the matured ("aged") clay thus consist of rather large stacks ("domains") of face-to-face-grouped montmorillonite lamellae, which have been referred to as "quasicrystals". Their average orientation in bulk clay is at random.

On wetting, water is assumed to be sucked up by the system of interconnected inter-aggregate voids by "capillary action" and this water is then redistributed to the interlamellar space which expands on expense of the interaggregate voids. In the ultimately developed microstructure a certain fraction of the porewater, the "external water which is unaffected by the minerals, is contained in these voids while the remaining fraction is the interlamellar, "internal" water, which is strongly associated with the minerals. Since there should be a very significant difference in physical properties of these two water types we naturally require a quantitative estimation of their mass ratio for evaluation of the rheological properties of the clay in bulk. This matter is dealt with in the subsequent chapter.

2.3.2 Internal and external water

The evaluation of the relative amounts of internal and external water is suitably based on detailed microstructural analyses which require microtome sectioning and transmission electron microscopy (7). Such studies have demonstrated that the clay matrix of smectite-rich materials holds internal water, the amount of which is related to the external water in a fashion that is largely determined by the bulk density (4). The porewater chemistry is also a determinant according to classical colloid chemistry as illustrated by the fact that an

increase in ion strength produces coagulation of particles by which the ratio of internal and external water is diminished. The latter effect, resulting from electrical double interaction and attractive mass forces between the stacks, is not significant at bulk densities exceeding about 2 t/m^3 but is certainly important at densities lower than about 1.5 t/m^3. For any particular pore water salinity there is a unique relationship between internal and external water. Data derived so far suggest a relationship of the type shown in Fig 5.

Fig 4. Schematic particle arrangement in dense bentonites: Left: Compressed granules (A) with inter-aggregate voids (a) and interlamellar space (c). Right: Homogeneous, water saturated state with expanded granules forming stacks, the voids being smaller and the interlamellar space being wider than in the initial state
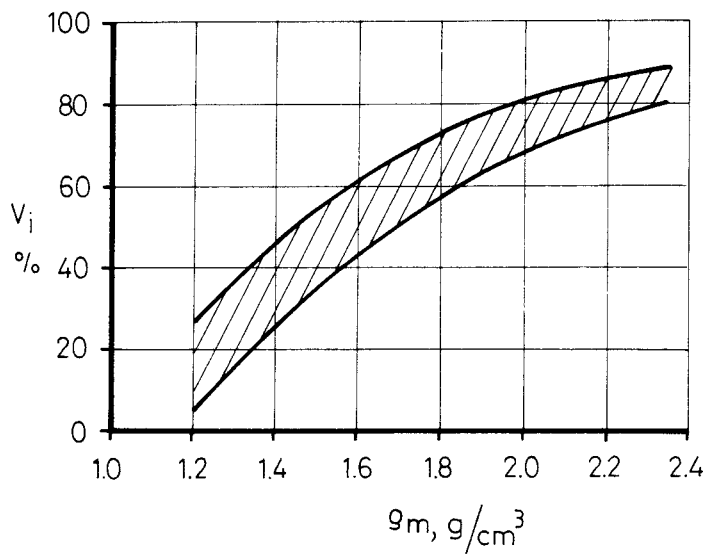
Fig 5. General relationship between bulk density and content of internal water in percent of the total pore water volume of smectite clays (4)

3   SETTLEMENT OF CLAY-ENVELOPED CANISTERS

3.1   Physical processes leading to settlement

Prediction of the settlement of foundations resting on clay is a classical problem in soil mechanics. There is no deep understanding of the involved mechanisms and the usually applied model is simply that the settlement is mainly caused by compression of clay elements in which the preconsolidation pressure is exceeded. This pressure, which is understood as the maximum effective pressure caused by the overburden under which the clay has reached a condition of equilibrium - possibly in conjunction with chemical effects like precipitation of cementing substances - is usually different in the vertical and horizontal directions. This means that deviator stresses prevail in the consolidated clay and that a load increment produces a collapse of the particle network, which ultimately reaches a new state of equilibrium with a denser grouping of the particles. The compression is delayed because of two effects: 1) the permeability, which is usually low, does not allow pressurized porewater to be expelled rapidly, and 2) the stress/strain properties of the particle network becomes a determinant of the compression rate when the induced hydraulic gradient has dropped to a low value. The initial part of the compression, i.e. the primary consolidation in which the porewater overpressure dissipates, has the character of diffusion and yields the S-shaped part of the curve in Fig 6, while the subsequent compression in which there is no porewater overpressure is characterized by an almost straight curve in log time representation. Various investigators have demonstrated that the deformation properties of the particle network may alter the shape of the primary consolidation curve and it may be difficult to distinguish between the primary and secondary phases only by watching plots of the type shown in Fig 6.

In addition to the compression, the clay mass will undergo shear-induced strain and this contribution to the settlement is dominant in overconsolidated clays, i.e. soils in which the preconsolidation pressure is not exceeded.

The two major mechanisms that yield macroscopic displacement of clay-enveloped canisters are schematically illustrated in Fig 7.
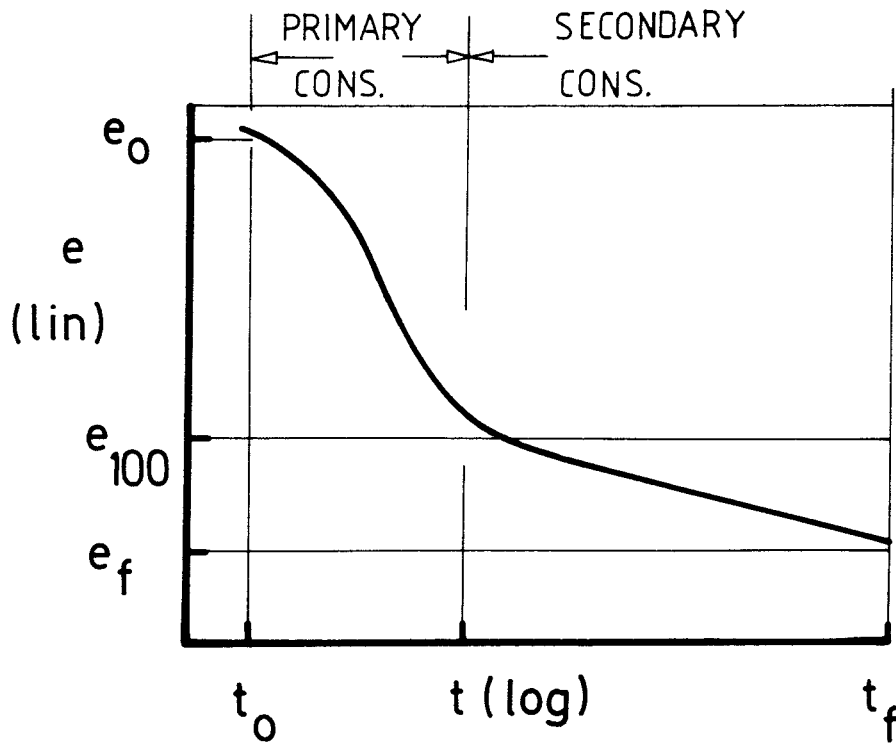
Fig 6. Time-dependent decrease in void ratio in primary and secondary consolidation. e_o is the void ratio at time t_o, while e_{100} is that at 100 % primary consolidation
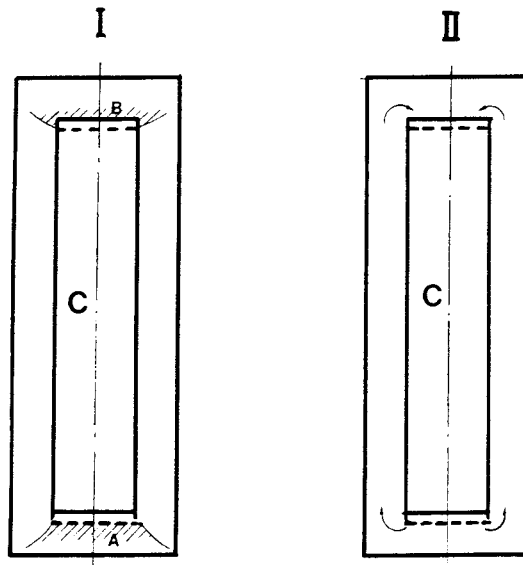
Fig 7. Possible settlement-producing mechanisms. I) Consolidation by compression of zone A and swelling of zone B, and II) Viscous, fluid-like flow under constant volume conditions. C is canister

3.2   Settlement due to consolidation of dense Na montmorillonite

3.2.1 Consolidation properties

Dense Na montmorillonite deviates markedly from clays composed of other minerals in that it has a very strong ability to become homogeneous by internal redistribution of water and solids. This fluid-like behavior, which is manifested by a very low angle of internal friction, means that the swelling pressure is isotropic and can be considered as a preconsolidation pressure.

This would imply that all the clay elements in a deposition hole with a heavy canister tend to stay homogeneous with no local compression, which in turn would yield a fluid-like displacement of the clay with concomitant settlement of the canister. However, considering that the microstructure allows for a certain strain by displacement of the quasicrystals and expulsion of external water without any change in internal water, it is concluded that some true consolidation in the form of local compression will take place in the deposition holes.

3.2.2 Estimation of consolidation settlement

The swelling pressure is empirically related to the bulk density and water content as shown in Fig 8, from which we can see that this pressure is just about 8 MPa for a bulk density of 2.05 t/m^3, i.e. the value often referred to as a suitable ultimate bulk density of the KBS 3 concept. Assuming now that the weight of the canister is transferred to the clay via its circular base, which would correspond to a condition of no friction or adhesion at the clay/canister interface, the average contact pressure 0.4 MPa would theoretically yield consolidation leading to an increase in bulk density by about 0.005 t/m^3 and a drop in water content by about 0.3 percent units. Since the average vertical pressure is transferred downwards without any significant reduction to a depth that is roughly equal to the radius of the canister (8), we find the settlement s caused by vertical compression of the clay to this depth to be described by Eq. 3:

$$s = 0.003 \ R \hspace{4cm} (3)$$

where R is the radius of the canister.

Putting R = 0.39 m, i.e. the size of the KBS 3 canister, we find the primary consolidation settlement s to be about 1.2 mm, while it would be 0.07 mm for a canister radius of 2.5 cm, which is the size of the model canister in a test that is fully described later in this report. The time required for development of the primary consolidation is determined by the distance from the loaded clay elements to the draining boundary, and by the hydraulic conductivity. Taking the diameter of the deposition hole to be twice the canister diameter and the hydraulic conductivity of the clay to be 10^{-14} m/s, we find that the primary settlement is fully developed in a few years in the full-sized canister case and in a few weeks for the model canister.

In practice, the canister load is likely to be transferred to the clay also via its perimeter. Assuming for the sake of simplicity, that the clay/canister interaction can be expressed in terms of wall friction characterized by the low friction angle 5°, we find the net load that would be transferred via the canister base to be negligible and no measurable consolidation settlement is actually expected.
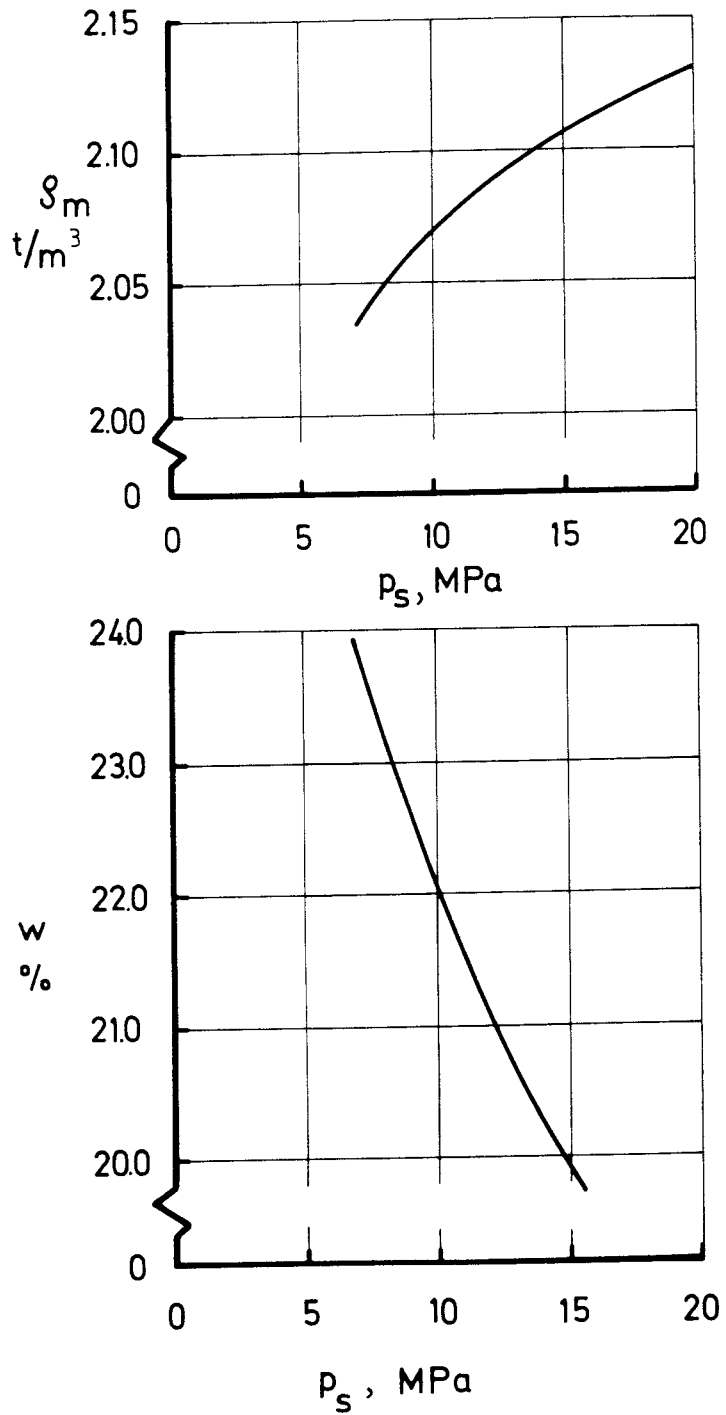
Fig 8. Empirical relationships between bulk density, water content, and swelling pressure of Na bentonite (MX-80)

3.3 Settlement due to shear-induced strain under constant volume conditions

3.3.1 Nature of creep strain

Shear-induced viscous flow like that of fluids, i.e. with no volume change, is expected to be the cause of time-dependent canister settlement in the absence of consolidation. It can be produced by creep deformation of the individual structural units and by a time-dependent rearrangement of these units. Since the individual montmorillonite flakes are separated by interlamellar hydrates, the stress/strain properties and interaction with smectite crystal lattices of the hydrates, are expected to be determinants of the bulk rheological behavior. In principle, macroscopic settlement of the presently discussed type is caused by accumulation of strain on a molecular level as will be briefly outlined here.

The Na montmorillonite quasicrystals composed of stacks of lamellae with internal water only, are expected to behave as elasto-plastic bodies if Forslind's hydration model applies and the organization of water molecules were perfect. However, the molecular disorder caused by the fact that natural as well as industrially processed Na bentonites have a significant fraction of bivalent cations in exchange positions and that crystal defects are numerous, imply that the activation energy for shiftings of single water molecules and patches of molecules is largely varying. This suggests that the individual "quasicrystals" and therefore also the integrated network of such units are characterized by a spectrum of activation energies for slip, the lower boundary of the spectrum (u_1) corresponding to weak hydrogen bonds (0.1 eV) and the upper one (u_2) to strong hydrogen bonds, electrostatic bonds or even primary valence bonds, i.e. 0.6 eV or higher (Fig 9). There are strong reasons to believe that the creep behavior of dense Na montmorillonite under deviatoric stress conditions is similar to that of illitic clays, but since direct crystal lattice contacts are very rare and the average activation energy for slip therefore lower than in illitic clays, the creep rate of the smectite clay would be expected to be much higher. However, the rather extreme homogeneity of dense Na montmorillonite clay compared to that of dense illitic clay would imply a narrow energy spectrum

and a much higher number of slip units in the first-mentioned clay, which in turn would yield weaker forces on each slip unit and therefore less creep strain at any given stress level. The counteraction of these two effects makes it difficult to predict the strain rate on pure theoretical grounds. The matter will be further discussed in the last chapter.
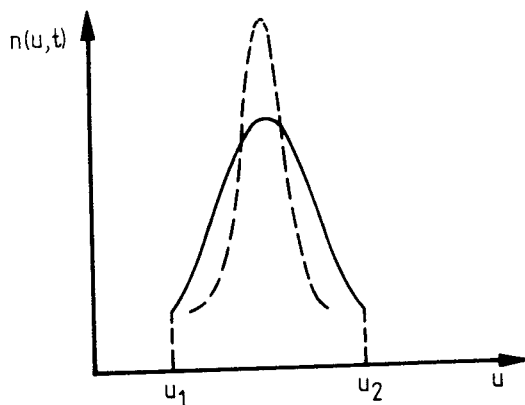
Fig 9. Activation energy spectrum at a given, short time t after the onset of creep. Full line represents aggregated clay with largely varying barrier heights u due to many kinds of particle bonds. Broken curve is typical of a more homogeneous clay with one dominant type of bonds

3.3.2 Estimation of settlement due to shear-induced flow

The long-term settlement of clay-enveloped radioactive canisters has been discussed in a couple of scientific articles. An early attempt concerned the mechanical response of clayey marine sediments due to subseabed emplacement of nuclear waste (9) and it was based on equations representing conservation of mass, momentum and energy, and on constitutive relationships for the sediment and porewater. The settlement was calculated with special respect to the time-dependent heat production of the canister (initially 3.4 kW), which was taken to have a diameter of 0.4 m and to be 3 m long. The approach was purely "viscous", i.e. the FEM calculation gave the motion of the canister by assuming the clay to flow around it, the constitutive equation being of the form:

$$\varepsilon = A \cdot D \cdot e^{-B/T} \cdot t \tag{4}$$

ε = strain of individual clay element

A, B = coefficients

D = deviator stress

T = temperature

t = time

The assumption that the settlement rate is proportional to the average deviator stress is an oversimplification which can still be accepted for low stress levels and for post-failure stages, while taking this rate to be constant with respect to the time makes the model too primitive to be of any practical value. This is particularly clear from the fact that the parameter values were picked rather arbitrarily from published laboratory investigations, and that the underlying physics was not discussed at all by the modellers.

In 1983, a general soil creep theory based on statistical mechanics and formulated with due respect to the microstructural constitution of clays (10), was used for predicting the settlement of the KBS 3 canister (11). The creep law, which allows for stress and temperature variations in a simplified way, has the analytical form given by Eq. (5) and Fig 10. Its physical basis will be discussed in a later chapter.

$$\dot{\varepsilon} = \beta TD \frac{1}{t+t_0} \tag{5}$$

where β = constant, T = temperature, D = deviator stress, and t_0 a structure-dependent term

Boundary element analysis was chosen to model the stress distribution in the clay surrounding the canister. This was then coupled to Eq. 5 to enable the time-dependent settlement to be predicted. This method is well suited to solving problems of this type because of its high accuracy, ease of use and ability to model incompressible and nearly incompressible materials accurately. The boundary element technique is derived from the equation of elasticity by first applying the technique of weighted residuals, or similar, to produce an integral equation:

$$\int_{\Omega} (\sigma_{jki}+b_k)U^*d\Omega = \int_{\Gamma_2} (\overline{P}_k - P_k)U^*d\Gamma + \int_{\Gamma_1} (\overline{U}_k - U_k)P^*d\Gamma \qquad (6)$$

where σ = stress, b = body forces, P = tractions, U = displacements, U* = weighting function, Ω = volume of problem, and Γ = surface area of problem.
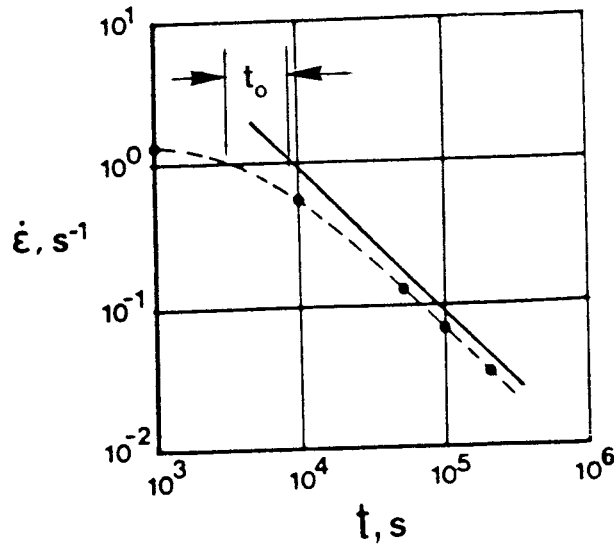
Fig 10. Creep curves according to Eq. (5), the full line corresponding to t_o=0

This can be manipulated to produce a set of equations involving only integrals over the surface or boundary of the problem. Because the method only requires the evaluation of integrals over the surface or boundary of the problem, the user of the program BEASY* has only to subdivide the boundary into elements. In the case of a two-dimensional or axisymmetric problem, the elements consist of lines.

----

* The "BEASY Users Manual" is available through CM BEASY, 125 High Street, Southampton, Great Britain

The strain-determining deviator stress is defined as follows:

σ_1 = the larger of the principal stresses in the r-z plane

σ_2 = the smaller of the principal stresses in the r-z plane

σ_3 = the hoop stress

$D = \sigma_1 - \sigma_2$

The settlement is obtained by integrating the axial strain ε from the bed rock to the base of the cylinder. Therefore:

$$s = \int_1 \varepsilon dl = \int_1 \beta TD \ln t \, dl \tag{7}$$

As $\beta T \ln t$ are constants in space:

$$s = \beta T \ln t \int_1 D dl \tag{8}$$

this equation will produce a different result depending upon which path l is taken. To resolve this problem an average settlement is calculated by integrating Eq. (8) over the base of the cylinder and dividing by its area. Thus:

$$s = \frac{1}{A} \int_o \int_1^R Ddl \, 2\pi dr \beta T \ln t \tag{9}$$

where A = area of the base of the canister, R = radius of the base of the canister, and s = average settlement of canister. Finally:

$$s = \frac{\beta T \ln t}{A} \int Ddv \tag{10}$$

where:

$$\int_v Ddv = \int_o^R R \, Ddl \, 2\pi dr \tag{11}$$

Taking t_o to be zero, which is admissible for high t-values, and introducing β-values derived from undrained triaxial creep tests, the predicted settlement was calculated for the two canister sizes considered earlier in the text, i.e. the KBS 3 canister with R = 390 mm and a model canister with R = 25 mm. The results are given in Table 1 for the case of non-slip along the rock/ clay interfaces.

Table 1. Predicted settlement in millimeters as a function of time
for T = 295 K

Time,	Canister radius	
years	390 mm	25 mm
0.01	0.85	0.003
0.1	1.0	0.005
1.0	1.15	0.007
10	1.30	0.009
10^2	1.45	
10^6	2.05	

3.4 Remarks

We see from the preceding text that the shear-induced flow yields a settlement of the big canister after 10 years that is approximately 100 % of the value that primary consolidation would account for if slip takes place along the clay/canister interface. On the other hand, the movement of the model canister caused by shear-induced viscous flow is only about 10 % of the predicted primary consolidation. As demonstrated in the subsequent chapter, a laboratory short-term test with the model canister gave fair agreement with the values in the right column of Table 1 (11), which suggests that shear-induced strain under constant volume conditions, i.e. viscous-type flow, is the dominant physical process, supporting also the assumption of non-slip along the clay/canister interface. Since this agreement could be a coincidence by mere chance, the test was extended to run for about 1.5 years, which offered an excellent opportunity to analyze the involved physical processes and to get an overall view of the thermo-mechanical behavior of the integrated clay/canister/confinement system.

4   EXPERIMENTAL

4.1   General

The long-term settlement of a copper canister surrounded by water saturated Na bentonite was investigated in a small-scale test that was planned and prepared in late 1984 and early 1985, and conducted in the period April 1985 to December 1986. It involved saturation of the clay before a dead load was applied, which thus differs from the conditions in a real repository where the load is in operation when the saturation begins.

The test was conducted at room temperature except for two periods when the ambient temperature was raised to 50 and 70°C, respectively.

4.2   Test setup

The experiment was carried out with the device shown in Fig 11 using highly compacted bentonite (MX-80) with a theoretical density at saturation of 2.07 t/m^3, which corresponds to a water content of about 22.0 %. The inserted blocks were wetted by keeping the circumferential filter water-filled until saturation was achieved, after which a dead load of 80 kg, resulting in a contact pressure of 0.4 MPa at the base for the theoretical case of slip along the clay/canister interface, was applied instantly at the lower end of a $\emptyset$ 3 mm copper rod that was connected to the canister and passed through teflon bushings in the base and top of the container. The resulting settlement, which was developed under drained conditions, was recorded by means of an inductive strain gauge with a sensitivity of 10^{-4} mm (Fig 12). The high accuracy of the gauge could not be utilized without careful temperature measurement and control, the accuracy of the evaluated settlement being estimated at 0.1 μm. A mechanical precision dial gauge was used as back-up.

The steel container, which represented the rock surrounding a deposition hole, was rigid in order to minimize displacements of the outer boundaries of the clay. The known heat-induced expansion of the container made it possible to evaluate the major features of the thermo-mechanical behavior of the clay/canister/container system.

The 2.5 mm thick filter was made of sintered polyethylene (PIAB) with an E-modulus of about 100 MPa and a maximum pore size of 0.09 mm.

4.3 Test program

The major stages of the test were those specified in Table 2.

Table 2. Test program

Activity	Temperature, °C	Time
Application of dead load		April 22, 1985
First "room temperature" period	21.5-22.0	April 22-July 6 1985
First heating period	~50	July 7-July 29 1985
Second "room temperature" period	17.5-23.0	July 30 85-May 13, 1986
Second heating period	~70	May 14-Sept 29 1986
Third "room temperature" period	20.3-22.0	Sept 30-Dec 15 1986
Dismantling for comprehensive water content determination and analysis	-	Dec 15-Dec 20 1986

In the first heating period the air temperature of the test chamber was increased to 50°C by using a heater and an effective fan for air circulation through which the temperature could be maintained in the narrow temperature interval 49.5-50.1°C. Heating to 70°C required rearrangement of the test by applying a heat coil and a thermostat which kept the outer wall surface of the heat-insulated steel container at the required temperature. By this the temperature variations were confined to the interval 69.6-69.9 °C during the more than 4 months long test.

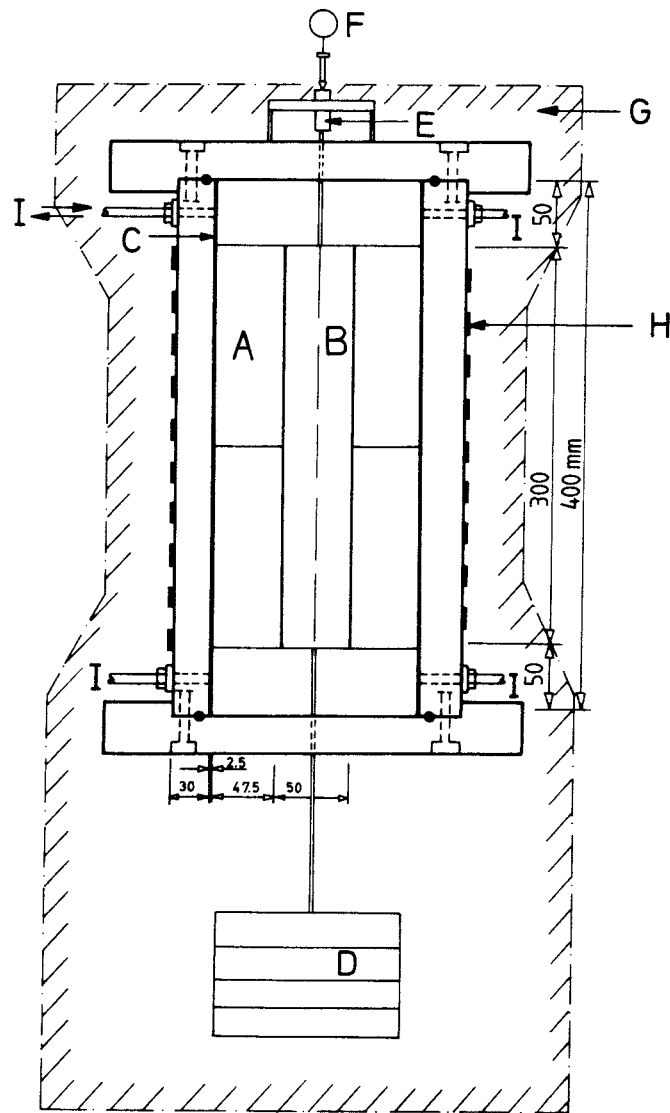Fig 11. Test device. A) Bentonite blocks, B) Copper canister, C) 2.5 mm filter, D) 80 kg dead weight of lead, E) inductive strain gauge, F) mechanical dial gauge, G) heat insulation, H) heat coil, I) drainage tubings
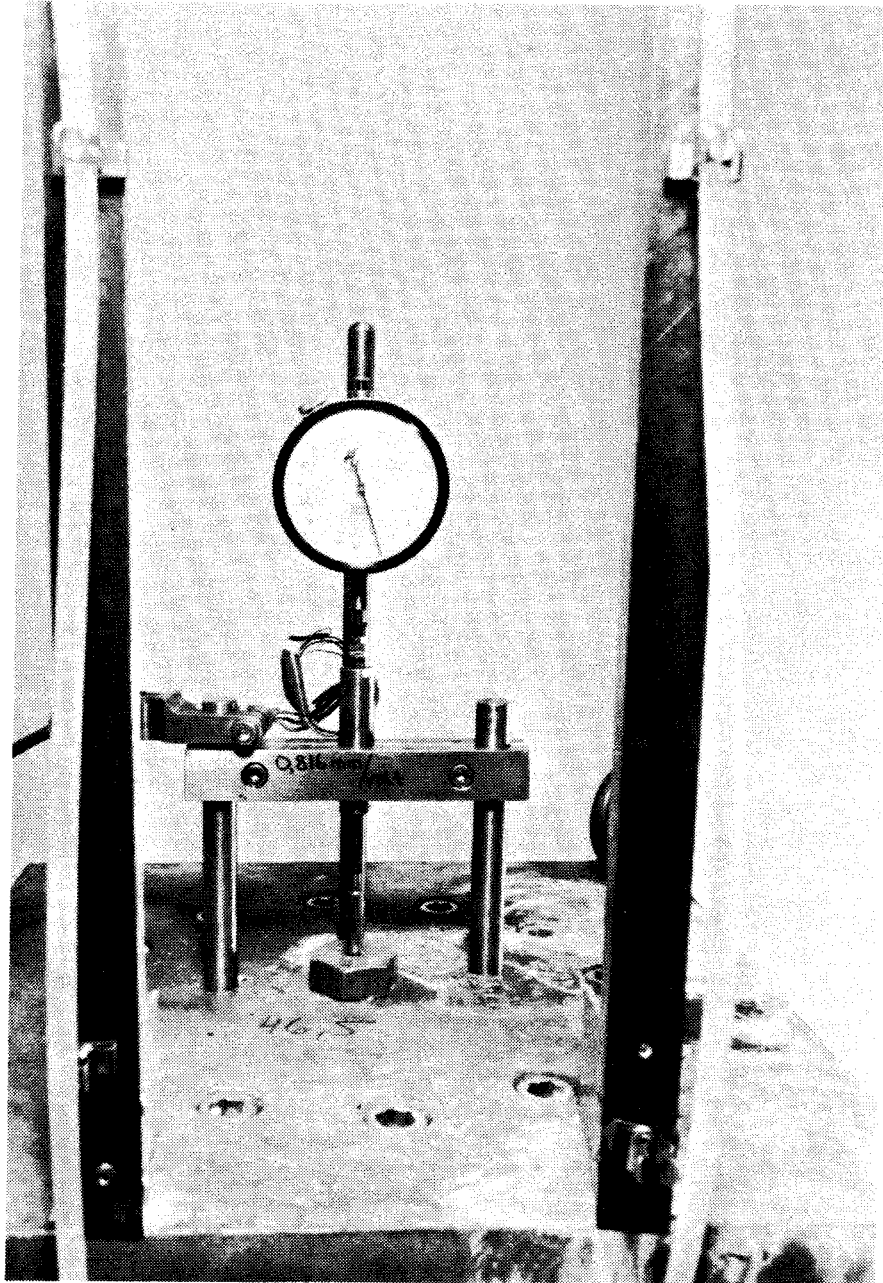
Fig 12. Gauges for measurement of the canister settlement. The nylon
tubings, each with a water meniscus in the foreground, served
as drainages from the filter that surrounded the clay

4.4   Clay preparation

Blocks were prepared from larger units that were left over from the Buffer Mass Test in Stripa. They were given the desired, regular shape by sawing and trimming with a sharp knife. The initial water content of these blocks, which had been equipped with tightly fitting plastic covers during the storage in Stripa, was 10-13 % but during the preparation it rose to about 14 %.

The isostatic compaction of the MX-80 Na bentonite clay powder that had been made in the preparation of the Stripa material would imply precisely the microstructural features shown in Fig 4. Only the material in the close vicinity of the joints of the blocks may have had a different structure imposed by the manufacturing. Here, the fabric may possibly have been characterized by an overall alignment of the montmorillonite stacks by which the amount of external water may have been smaller and therefore the average water content slightly lower than in the interior parts of the blocks.

4.5   Water saturation

Distilled water was used for saturation, the required time of which being predicted by a FEM analysis using an 80 element axisymmetric model and the water-uptake model derived by Börgesson (12). It implies that the water content gradient is a determinant of the migration rate and that this rate can be expressed in terms of a diffusion process when the clay density is high, the D-coefficient being $3 \cdot 10^{-10}$ m^2/s. Thus, the equation has the form in Eq. (12):

$$\frac{\delta w}{\delta t} = D\nabla^2 w \qquad\qquad (12)$$

where w = water content
    t = time after onset of water uptake
    D = diffusion coefficient

The calculated total amount of water for complete saturation was 2.1 liters, which was also the measured quantity after almost 3 months. The initial water content was taken as 14 % and the ultimate one as 20 %, which was slightly lower than the actual value. The increase in

water content of the node that had the slowest wetting rate is shown in Fig 13, from which we see that almost complete saturation would be expected after 2.5 - 3 months.

As mentioned earlier in the report, montmorillonite flakes and water are expected to be redistributed so that all elements of a clay that is microstructurally isotropic become equally dense and exert the same isostatic pressure in the ultimately achieved state of equilibrium. This implies that the water content is constant throughout a matured montmorillonite clay mass with an isotropic microstructure when the mass is at rest. However, impurities in the form of non-swelling minerals and the presence of inter-aggregate voids which may be non-uniformly distributed, are assumed to cause some variation in water content of the saturated but not yet loaded clay. A major question to be answered by the experiment was therefore how uniformly the water is actually distributed in virtually homogeneous, dense smectite, and also if Eq. (12) is valid when the degree of saturation exceeds 90-95 %.
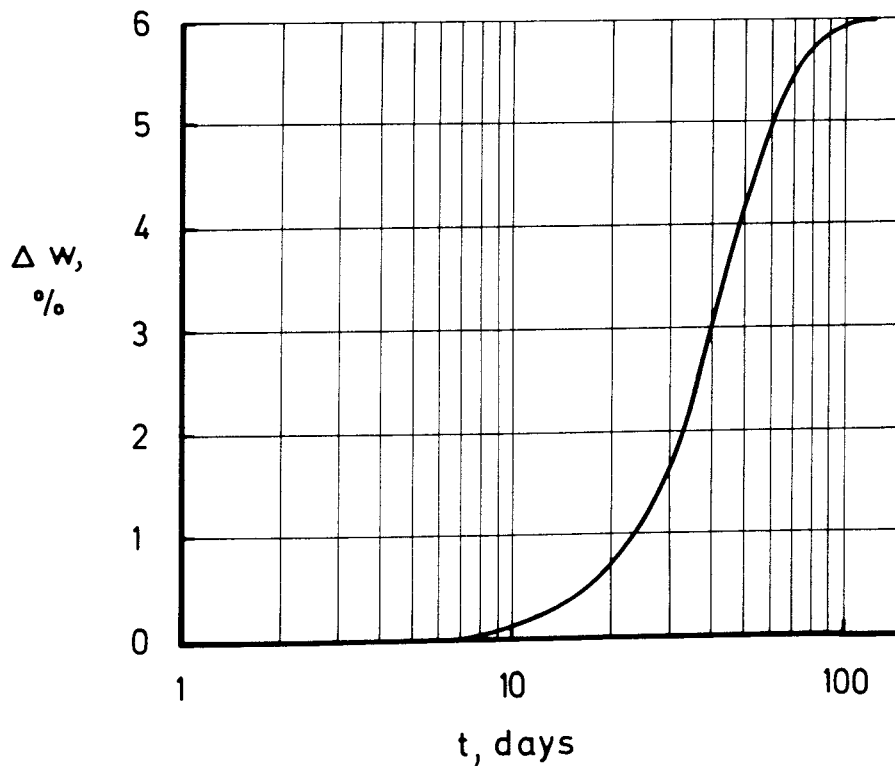
Fig 13. Calculated increase in water content of the node that had
         the slowest wetting rate

4.6   Test results

4.6.1   Major characteristics of the settlement progress

Fig 14 shows the entire settlement sequence plotted as a function of time using linear scales and introducing appropriate temperature corrections. It is immediately seen that the settlement was very small in the "room temperature" intervals as well as at elevated temperature, while relatively large movements took place in the first day after each temperature change. These movements mirror the thermo-mechanical behavior of the integrated system of the container/filter/clay/canister and have nothing to do with the intrinsic strain properties of the clay at constant stress conditions. Still, they are of importance to the overall behavior of the clay-enveloped canister and will therefore be discussed in the first place.
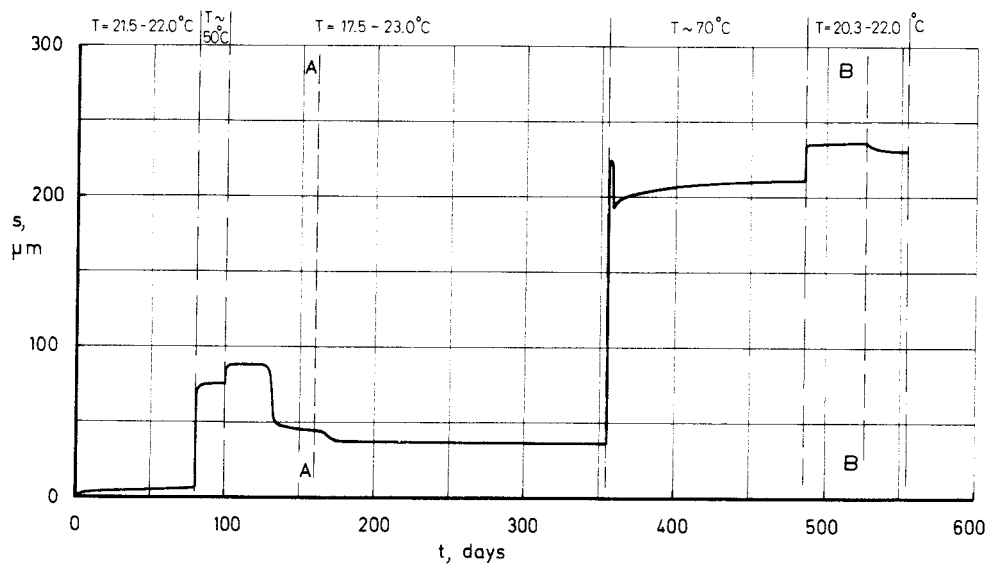
Fig 14.   Evaluated settlement. A and B represent occasions when the water inlets I in Fig 10 had been cleaned and increased in number, respectively

4.6.2   Thermo-mechanical processes

While temperature variations in the range of about 20-22°C had short duration and did not influence the movement of the canister in a measurable way, the heating to and from 50 and 70° C, respectively, had a significant influence. The predicted, main short-term effects were the following:

On heating:

* Stage 1: Instant heat-induced expansion of the steel casing will take place, by which the confinement of the clay is temporarily reduced. The canister continuously exerts pressure on the underlying clay which will thereby be displaced downwards and laterally, causing the canister to settle.

* Stage 2: The heating of the clay makes it expand and exert an increased pressure on the filter C in Fig 11. The filter is thereby expected to be compressed radially, the compression being slightly larger below the canister where the thermally induced pressure is superimposed by that generated by the canister load. The induced porewater overpressure will cause consolidation of the clay, which should be manifested by observable water expulsion.

* Stage 3: After development of isothermal conditions and completion of the thermally induced consolidation, the canister will continue to settle.

On cooling:

* Stage 1: Instant contraction of the steel casing will cause additional rapid compression of the filter, particularly above the base of the canister where the filter may previously have been less compressed than below. This could possibly yield an instant slight upheaval of the canister.

* Stage 2: Thermally generated contraction of the clay, causing a reduced lateral pressure will make the filter expand.

Assuming that it had been more compressed in the lower part, the elastic expansion that follows from the pressure release will yield upheaval of the canister but this movement will be counteracted by the creation of an anisotropic stress state in the clay below the canister. Here, the reduced lateral stress and the largely preserved vertical stress will lead to downward displacement of the clay and hence settlement of the canister. In the first few weeks these processes may balance each other and no settlement may be developed. Soon after turning off the heat the stronger contraction of the clay than of the steel casing initiates water uptake and swelling so that the physical state of the preheated clay is ultimately regained.

The evaluation of the practical importance of these effects and the possibility of identifying them, required determination of the rate of heating of the individual components. This was made by applying the same FEM program that had been used for predicting the saturation process, the presently applied parameters being specified in Table 3.

Table 3. Temperature-related properties of the canister settlement units

Material	Heat conductivity W/m, K	Heat capacitivity Ws/kg, K	Bulk density kg/m^3
Copper	380	390	8930
Sat bentonite clay	1.4	1600	2100
Filter	0.5	4200	1000
Steel casing	59	460	7800

The calculation showed that heating of the entire system from room temperature to 50°C would take place in about 5 hours (Fig 15). Thus, the effects of the expansion or contraction of the steel casing prior to heat-induced changes of the interior parts would appear in the first 0.5-1 hours after altering the surface temperature of the casing. As demonstrated by Fig 14 the foreseen short-term settlement on heating as well as on cooling actually took place rapidly, thus

supporting the predicted thermo-mechanical scenario. The slow, long-term settlement following directly after the initial large movement appeared to be steady and related to some time function in the case of heating as discussed in the subsequent text, while there seemed to be no canister movement at all in the first few weeks in the cooling events. The tubings connected to the filter turned out to be clogged by clay that had been extruded in the consolidation phase of the heating, and after cleaning them (A in Fig 14) and increasing their number from 2 to 4 (B in Fig 14) some slight upheaval of the canister took place. This suggests that the preceding consolidation had caused a higher density in the lower part of the clay and that this part expanded and raised the canister when swelling finally took place, which is in principal agreement with the predictions.
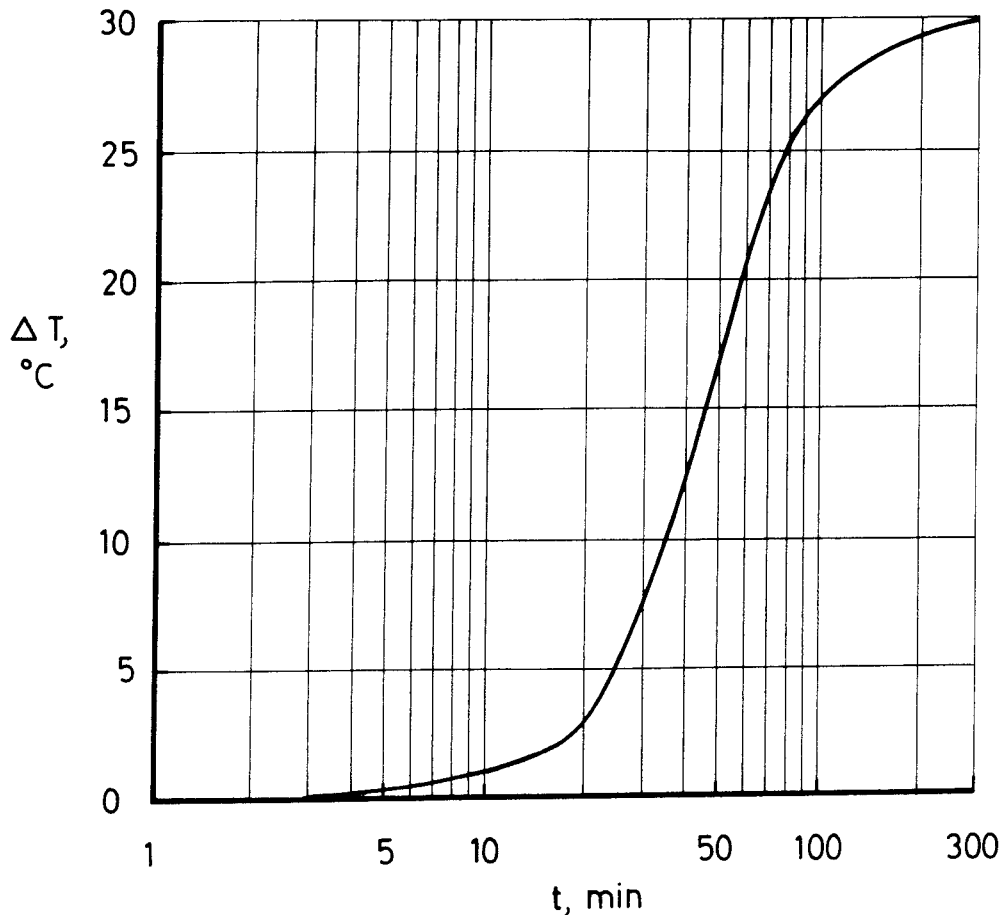

Fig 15. Temperature increase of the copper canister as a function of time after increasing the surface temperature of the steel casing

The involved volume changes and induced pressures can be evaluated from simple calculations based on available thermal expansion data of

the various components. Thus, considering heating from 20°C to 70°C we find that the volume of the steel casing increased by about 7.9 cm^3 from the original 6605 cm^3, while the solid mineral substance and the water expanded by 1.7 and 49.4 cm^3, respectively. Considering also that the copper canister expanded by 1.4 cm^3 we find that the components hosted by the casing expanded 44.2 cm^3 more than the casing. Most of this expansion was consumed by the peripheral filter, which had a original total volume of about 450 cm^3 and which is assumed to have been precompressed from 2.5 to 2.3 mm thickness under the action of the swelling pressure. Thus, the filter only had to experience a radial compression of another 0.2 mm to absorb the expansion. The corresponding porewater pressure that was produced would thus be on the same order of magnitude as the swelling pressure of the non-heated clay, i.e. about 8 MPa.

These calculations, which are approximations since the strain of the steel casing and the compression of the water were neglected, indicate that the compressible filter, serving as an elastic spring, must have played an important role in the complex thermo-mechanical interaction of the components. In this context it should be pointed out that the compression of the filter probably reduced its permeability which may have contributed to the delayed water inflow in the post-heating periods.

4.6.3   Analysis of the time-dependent settlement curve

4.6.3.1   First "room temperature" period (0-78 days after test start

A closer analysis of the settlement revealed that the log t creep law applied in the first 2.5 months long "room temperature" period, the total strain being 6 µm (Fig 16). The sudden application of the dead load caused a strain of 2-3 µm in the first few hours, mainly through visco-elastic deformation of the integrated system of casing, filter and clay. The shape of the settlement curve as well as the very small displacement indicate that consolidation by water expulsion was insignificant, while the agreement with the predicted flow-type settlement (cf. Table 1) is excellent. Still, part of the settlement may have been due to true consolidation although it was masked by the major flow process.

4.6.3.2 First heating period (78-100 days after test start)

After the initial complex thermo-mechanical processes involving consolidation, which appeared to have ceased approximately 1 week after the temperature increase, the settlement again proceeded according to the log t creep law (Fig 17).

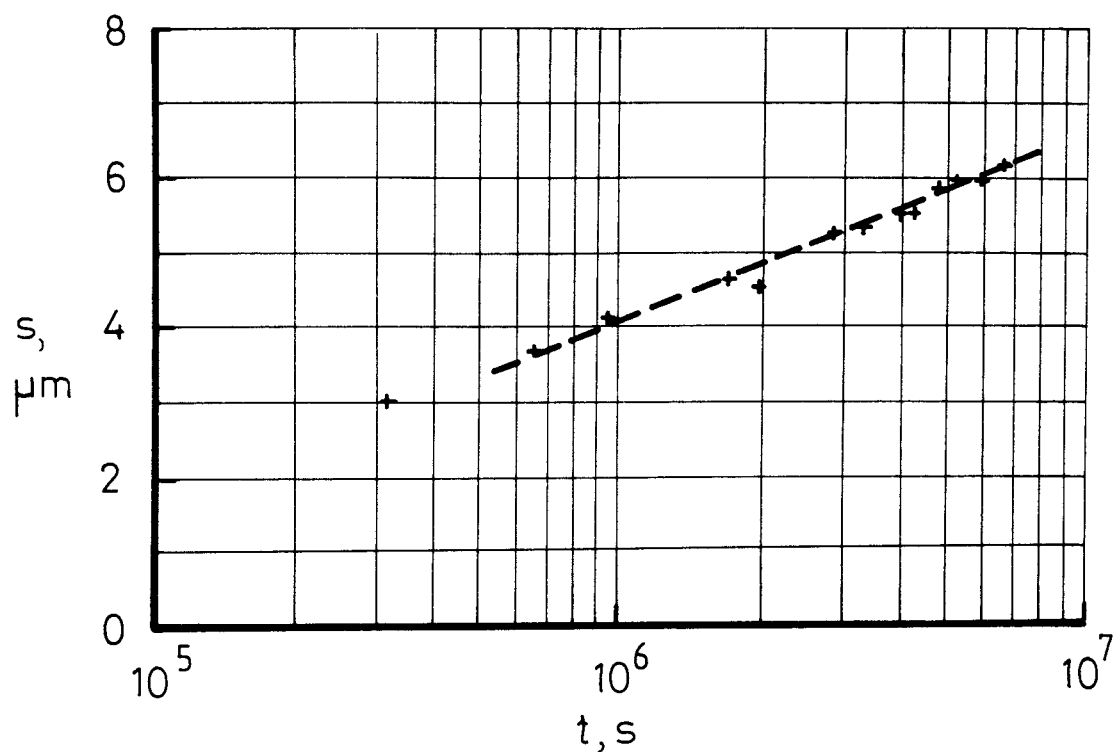Fig 16. Recorded settlement of the model canister in the initial period (T=21.5-22.0°C)

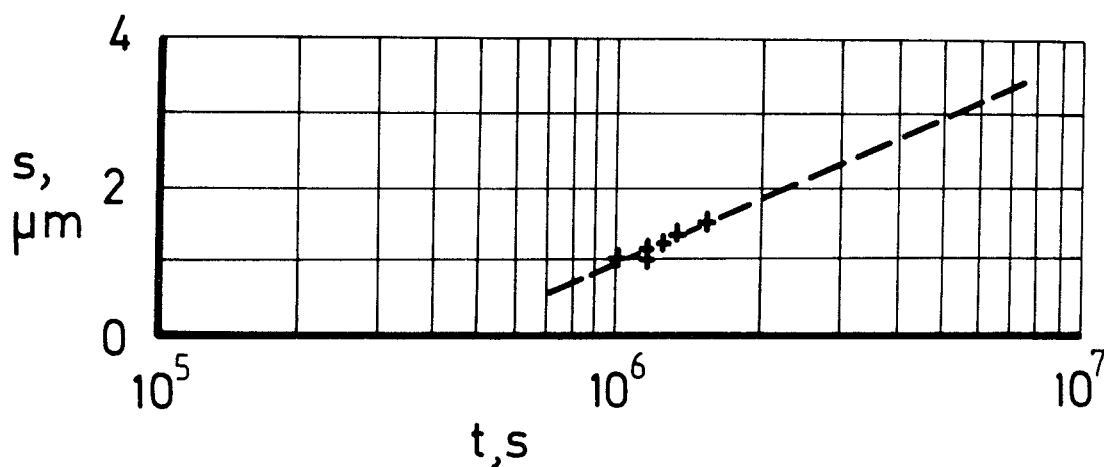Fig 17. Recorded settlement of the model canister in the first heating period (T ~50°C). The plottings concern post-consolidation conditions

Extrapolating the curve we find the settlement to be about 2.75 µm per decade, which means that the settlement proceeded approximately along the "virgin" curve in Fig 16 after the thermo-mechanically induced discontinuities. The short observation time in this first heating period does not allow for a very accurate evaluation of the influence of temperature on the creep rate, but comparison of the inclination of the curves for 22 and 50° C, respectively, suggests that the assumed proportionality specified in the basic Eq. (5) is reasonable for relatively low temperatures.

4.6.3.3 Second "room temperature" period (100-355 days after test start)

The thermo-mechanical processes completely governed the behavior of the system for about 1 week after turning the heat off and the water uptake that finally brought the clay back to equilibrium was delayed by several weeks due to clogging of the drainage tubings and, possibly, by a compression-induced reduction of the permeability of the filter. Thus, the movement of the canister, which actually had the character of slight upheaval, took place under transient conditions of the surroundings for approximately 5-10 weeks. Assuming that the reverberations of the thermo-mechanical processes had died out completely 15 weeks after turning the heat off, settlement of the canister under room temperature conditions was expected to take place from approximately 250 days after the start of the test (cf. Fig 14). However, the measurements unambiguously showed that no settlement occurred. The reason may simply be that the accuracy of the recording was not sufficient to identify the 0.3 µm settlement that would take place over the period 250-355 days provided that the "virgin" curve applies. Also, the preceding heating may have caused a "hardening" effect in the form of an improved structural ordering or, which is less probable, by an increased amount of dissolved silica that was partly precipitated in the subsequent cooling period. The matter will be further touched upon in a later chapter.

4.6.3.4   Second heating period (355-485 days after test start)

After the thermo-mechanically determined behavior in the first week after raising the temperature to 70°C, the settlement again appeared to increase according to the log t creep law (Fig 18). Thus, in the first two weeks this law applied while the settlement tended to be more retarded later in the test. The deviation from the log t law is certified since great care was taken to keep the temperature constant (69.6-69.9° C) in the more than 4 months long test period. If the "virgin" curve were applicable, the settlement in the second heating period would theoretically be only about 0.25 µm, which would correspond to about 0.3 µm if the linear temperature dependence of Eq. (5) is valid. The fact that the recorded settlement in the post-consolidation period actually amounted to about 12 µm shows that the temperature influence is significant and much stronger than implied by Eq. (5). However, the tendency of the settlement to be retarded beyond the log t-relationship does not permit evaluation of the long-term behavior at elevated temperatures.
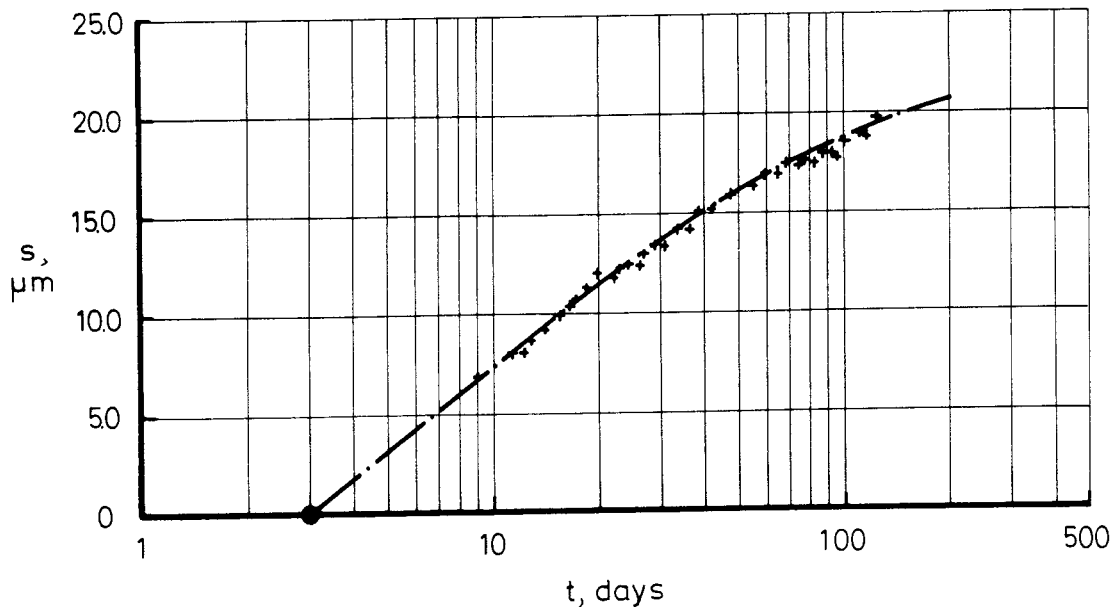

Fig 18.   Recorded settlement of the model canister in the second heating period (T 70°C). The plottings cover the post-consolidation stage

4.6.3.5   Third "room temperature" period (485-555 days after test
           start)

As in the preceding cooling periods, the canister rose when water was
finally absorbed by the clay. The upheaval was still going on at a
very low speed when the test had to be terminated and it is therefore
not known whether this ongoing upward movement would have been re-
placed by settlement when more than 2-3 months had passed after
turning off the heat.

4.6.4   Analysis of the water content distribution after termi-
           nation of the test

4.6.4.1   General

The purpose of determining the water content distribution was to
investigate whether systematic differences in density existed at the
end of the test, particularly between the clay zones immediately
below and above the canister. As concluded from Chapter 3.2.2 the
water content of the clay below the canister base should be no more
than about 0.3 percent units lower than the average value of the mass
if consolidation had taken place due to the load. Naturally then, the
determination of the water content had to be made with an accuracy
better than 0.1 percent unit to allow for evaluation of the influen-
ce of consolidation.

4.6.4.2   Determination of water content

The applied procedure was to take samples weighing about 25 g and
immediately put them in small plastic boxes until drying at 105° C
took place, the intermediate storage being shorter than 10-20 mi-
nutes. After the drying, which lasted for about 24 hours, the samples
were weighed within 2 minutes. With this procedure and by use of an
automatic precision balance the estimated accuracy of each individual
determination was concluded to be within the interval ±0.1 percent
units.

Fig 19 illustrates sampling stages.
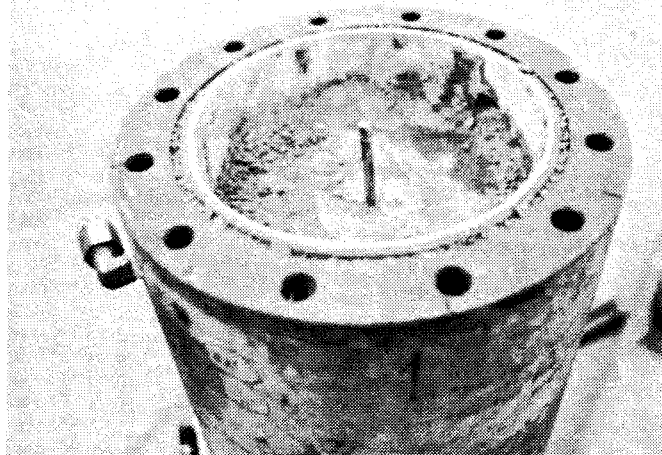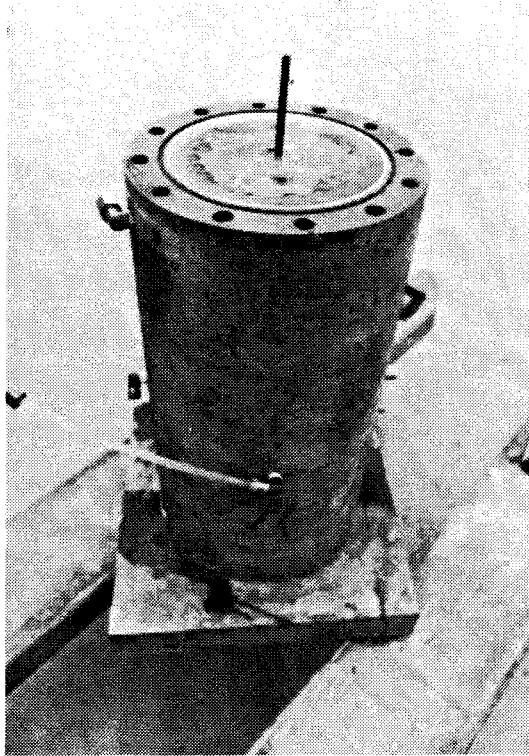
Fig 19. Excavation and sampling of the clay. Upper: The upper lid
has been removed and excavation is about to start. Lower:
The excavation has reached the upper end of the canister

4.6.4.3 Distribution of water in the clay

In total, 98 samples were taken from levels A-I located as shown in
Fig 20, i.e. with 5 cm spacing in the axial direction. At the end
levels A and I, and at mid height of the canister, level E, samples
were taken so as to demonstrate the radial distribution of the water
content (a to e).

We see from Fig 20 that the water content range was rather narrow, the extremes being 21.5 and 24.2 %, respectively, and the average value for the individual levels ranging between 21.7 and 23.3 %. This shows that the clay had been able to become largely homogeneous despite the various thermo-mechanical sequences that it had under-gone. It is obvious, however, that redistribution of water and solids to reach completely isotropic conditions had not taken place and we probably have an illustration of how far homogenization can proceed in dense Na montmorillonite, meaning that differences in water con-tent on the order of about 1 percent unit will never be evened out. It is of particular interest to see that the three determinations of the radial distribution of water all show slightly higher contents at the outer periphery than at the center. This may reflect the condi-tions at the last "room temperature" test phase in which the clay expanded by taking up water from the filter. Here the clay had been wetter from the start of the expansion period and complete homogeni-zation may not have been achieved yet, and would probably never be arrived at either.

Separate determinations at the top of the canister on the B-level and just below it on the H-level are of significant interest. Fig 21 shows that the latter is 23.11 %, which is actually slightly higher than the water content 22.67 %at the upper end of the canister. Both figures are very close to the average value for the respective level, which supports the earlier conclusion that consolidation has not taken place to a measurable degree under the applied canister load.

Level/ position	1	2	3	4	5	6	7	8	w	σ_n
A	22.4	23.3	22.7	22.8	22.6	22.9	23.1	22.6	22.8	0.27
B	22.3	22.1	22.7	22.7	22.7	22.7	22.8	22.7	22.6	0.23
C	21.8	21.9	22.1	22.1	22.1	22.1	22.3	22.0	22.1	0.14
D	21.6	21.5	21.7	21.8	21.8	21.8	22.0	21.7	21.7	0.14
E	21.6	21.5	21.8	21.8	22.3	22.0	21.8	21.7	21.8	0.23
F	22.2	22.2	22.7	22.5	22.6	22.6	22.6	22.3	22.5	0.19
G	22.5	22.5	22.8	22.5	22.4	22.5	22.5	22.4	22.5	0.12
H	22.7	23.1	23.2	22.8	22.6	23.2	23.1	22.8	22.9	0.22
I	23.0	23.4	23.7	23.4	23.3	23.4	23.4	23.1	23.3	0.20

Level/ Position	a	b	c	d	e
A	23.0	22.7	22.6	22.3	22.2
E	22.4	22.0	21.8	21.4	21.8
I	24.2	23.8	23.6	23.4	23.2
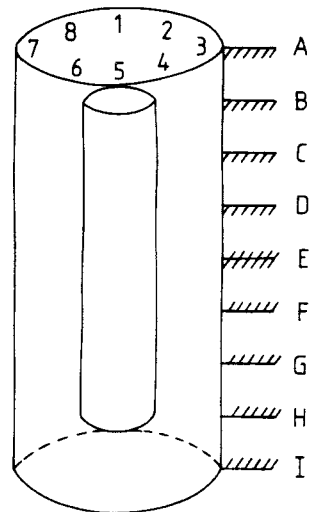
Fig 20. Water content distribution in the clay samples. w represent average values and σ_n the standard deviation
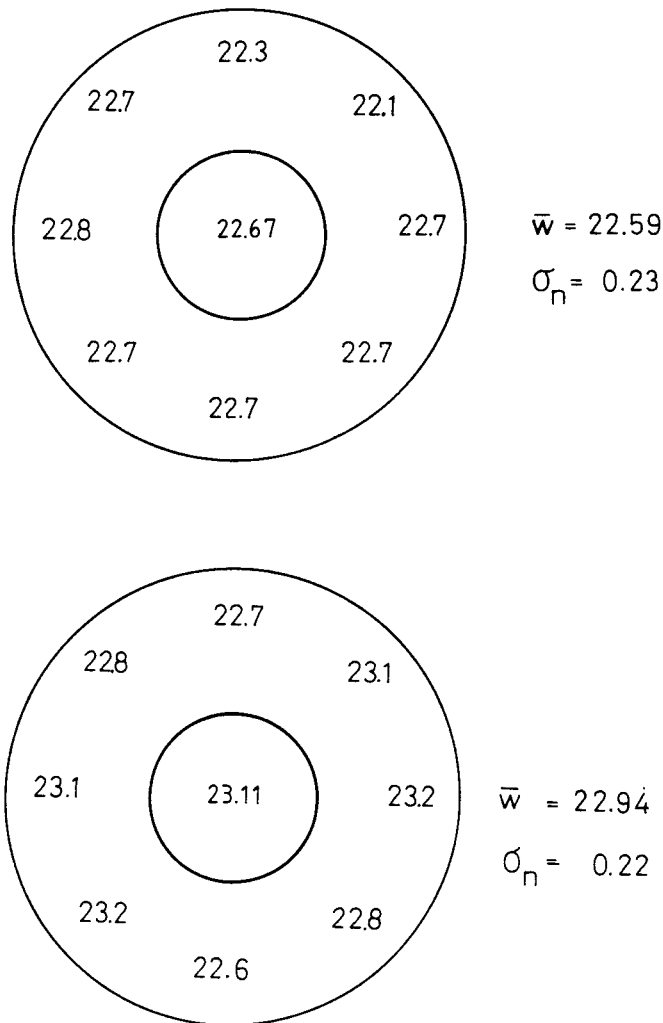
Fig 21. Distribution of water contents at the top level of the
canister (upper diagram) and at its lower end

4.6.5 Additional

The relatively long testing time gave an opportunity to get a visual
impression of possible chemical interaction between the bentonite and
the copper. The canister had the usual lustreless, red/brownish
appearance of copper at the application and it turned out to have
retained this property at the excavation. Thus, there was no indica-
tion of corrosion or other processes that could be seen by ocular
inspection.

5   DISCUSSION AND CONCLUSIONS

5.1   General

Apart from the thermo-mechanical behavior of the integrated casing/ clay/canister system, which was responsible for the large "instant" settlement and upheaval of the canister on temperature changes, the detailed shape of the time-dependent settlement curves under isothermal conditions are of primary interest. The discussion will be confined to the latter issue.

5.2   Validity of log t-type creep laws with respect to the involved physics

5.2.1   The log t law

The conclusion from the test that the major process leading to settlement of the canister was shear-induced flow under practically constant volume conditions, and that the settlement rate decreased rapidly after load application and temperature changes, support the assumption that the macroscopically observed strain was the integrated movement of slip units on a molecular scale as implied by the Pusch/Feltham creep model (10) referred to in Chapter 3.3.1.

The basic features of this model, applied to dense smectite clays of the presently investigated sort, are the following:

1   The clay operates as a heterogeneous system with deformable, dense aggregates forming a network with pores that contain a clay gel of varying density.

2   Macroscopic strain results from the integrated movement of slip units. It has the character of activated jumps on a molecular scale in the form of shiftings of patches of atoms or molecules as single units along geometrical slip planes.

3   The slip process leads to interaction of bigger and stronger structural elements, by which local stress relaxation and an

increase in the heights of the energy barriers for subsequent activated jumps.

4   New links and particle bonds formed in course of the creep process tend to increase the height of the energy barriers.

5   Regional redistribution of stresses facilitated by slip produces local stress concentrations. This is equivalent to a decrease in the heights of the energy barriers.

The transient form of the creep for low and intermediate deviator stresses suggests that those mechanisms dominate which increase the energy barrier heights, and this leads to a time-dependent spectrum of energy barriers to shear as explained by the following reasoning.

The dwell time, θ, of a slip unit at a barrier of effective height u, is given by the Arrhenius rate equation:

$$\theta(u) = \frac{1}{\nu_D} \exp\left(\frac{u}{kT}\right) \tag{13}$$

in which u = the barrier height; ν_D = an atomic vibrational frequency of the order of 10^{12}/sec; k = Boltzmann's constant; and T = the temperature in degrees Kelvin.

At any given temperature only a limited energy spectrum:

$$u_1 \leq u \leq u_2 \tag{14}$$

will be of relevance, for with $u < u_1$ the dwell-times will be too short, and for $u > u_2$ too long, to be of practical importance.

If slip has been activated at a certain point in the clay, i.e., a barrier has been overcome, a contribution to the overall shear is made by the associated extension of the local slip-patch. In the model it is assumed that the next barrier to be encountered by the same spreading slip-zone will be either higher or lower by an average amount u. The number of potential slip units per unit volume of material held up a time t at barriers of height u, is $n(u,t)\delta u$. Fig 22 shows consecutive activation energy intervals of the spectrum

which is subdivided into equal intervals u. The time rate of change
of the number $n(u,t)\delta u$ of flow units in the u-interval, i.e, $(\partial n/\partial t)$
is determined on the one hand, by the outflow from the u-level into
the higher energy-interval $(1/2)$ n $(u,t)\delta u$ ν_D exp $(-u/kT)$ and of the
same number into the lower one as indicated, respectively, by the
right and left lower arrows. Similarly, the simultaneous influx is

$$\frac{1}{2}\, n(u\, -\, \delta u,t)\delta u\ \nu_D\ \exp\left(-\,\frac{u\, -\, \delta u}{kT}\right)$$

$$+\ \frac{1}{2}\, n(u\, +\, \delta u,t)\delta u\ D\ \exp\left(-\,\frac{u\, +\, \delta u}{kT}\right)$$

If all the separate contributions are added, one obtains

$$\frac{\partial n}{\partial t} = \frac{1}{2}\, \nu_D\ \left[n(u\, +\, \delta u,t)\ \exp\left(-\,\frac{u\, +\, \delta u}{kT}\right) - 2n(u,t)\ \exp\left(-\,\frac{u}{kT}\right)\right.$$

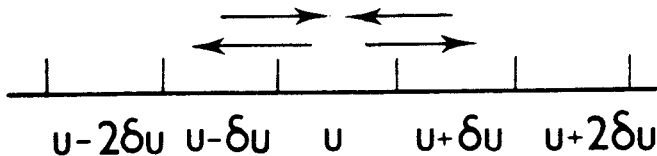$$\left. +\ n(u\, -\, \delta u,t)\ \exp\left(-\,\frac{u\, -\, \delta u}{kT}\right)\right]$$

Fig 22. Segments of activation energy range

Assuming that $\delta u \ll u_2 - u_1$, the right-hand side of the equation can
be seen to tend to the second partial differential of $n(u,t)$ exp $(-u/kT)$
with respect to u, as $\delta u \to 0$.

This yields, on writing n for n (u,t):

$$\frac{\partial n}{\partial t} = D \ \frac{\partial^2 \left[n \ exp \ \left(- \frac{u}{kT} \right) \right]}{\partial u^2}; \ D = \frac{1}{2} \nu_D \ (\delta u)^2 \qquad (15)$$

If each activated jump is taken to make the same, mean, contribution A* to the shear strain, , of the specimen, then the creep rate in shear will be

$$\dot\gamma = A^\star \int_{u^1}^{u^2} \nu(u)n(u,t)du = A^\star \nu_D \int_{u^1}^{u^2} n(u,t)exp \ \left(- \frac{u}{kT} \right) du \qquad (16)$$

The range of u-values terminates at u_1 at the low u end, while u_2 represents the upper limit of the operative spectrum. In the integration it is assumed that the scheme of jumps shown in Fig 22 is preserved at both ends of the cascade; thus u_1 is regarded as a "generating barrier", the formation of new slip units being favored in regions where the activation energies for slip are low. These new units are taken as providing the otherwise absent net inflow to the u_1-level. Again, jumps over barriers higher than u_2 will occur with such a low frequency that their contribution to the creep may be neglected and u_2 is therefore regarded as an "absorbing barrier".

The evolution of creep according to this model has been examined by numerical integration of the equations using discrete energy intervals in the thermally activated movement of independent slip units across energy barriers (13). The calculations were based on the assumption that the probability that a slip unit will have a kinetic energy sufficiently high to overcome a barrier encountered, is $e^{-u/kT}$ per attempt. If the attempt frequency of the slip units is ν_D, then the number of encounters in time Δt will be $\nu_D \Delta t$.

The probability, p, that a given unit held up at a barrier at time t, is still held up by the barrier at time t + t is therefore:

$$p = (1-e^{-u/kT})^{\nu_D \Delta t} \qquad (17)$$

If a large number of independent slip units are contained in independent potential wells of depth u, the fraction, f, which has crossed over during the interval t is:

$$f = 1 - p = 1 - (1-e^{-u/kT})^{\nu_D \Delta t} \qquad (18)$$

With a total of N steps δu we have $\delta u = (u_2 - u_1)/(N - 1)$. Activated jumps will be assumed to take a given slip unit, held up at a barrier of height u, with equal probability (1/2) to a barrier of height u + δu or u - δu. This single-step process characterizes the numerical-integration scheme which yields the distribution law, n(u,t), for the barrier heights. Here, we shall assume that n(u,0) = const for all u-values in the range.

Calculations have been made that cover the range of the hydrogen bond, an example being the diagram in Fig 23, which illustrates the aforementioned successive shift of the energy spectrum u_1 = 0.1 eV to u_2 = 0.6 eV from lower to higher values.

As to the creep rate, it is assumed in the theory that every jump makes the same contribution to the strain. The creep rate is thus obtained from the computed values of n(u,t) using the relation:

$$\dot{\gamma} \propto \sum_i n(u_i,t)e^{-u_i/kT} \tag{19}$$

Fig 24, showing the result based on Fig 23, demonstrates that the computed relation is of the type given by our basic Eq. (5), i.e. it yields a linear relation between the creep strain and the logarithm of time.
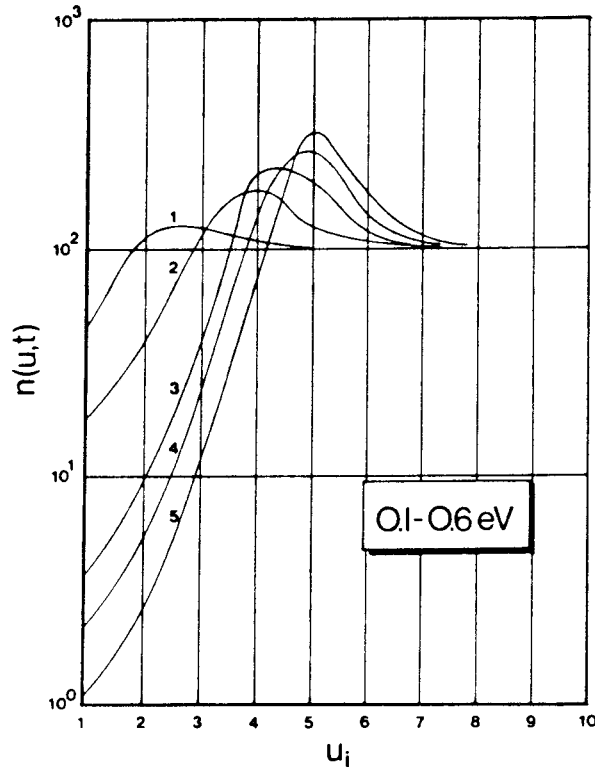
Fig 23. Number of slip units held up at barriers in each spectrum interval at different times after onset of creep (1) 10^3 sec: (2) 10^4 sec: (3) 5×10^4 sec: (4) 10^5 sec: (5) 2×10^5 sec (0.1 eV-0.6 eV). At t=0 the number of slip units held up per barrier interval was taken to be 100

Fig 24. Relationship between $\dot{\gamma} \propto \Sigma n(u_i, t) e^{-u_i/kt}$ and time, t, for 0.1 eV-0.6 eV (straight line is obtained on plotting $t+t_o$ with t_o = 7000 sec instead of t)

5.2.2   Influence of low shear stresses

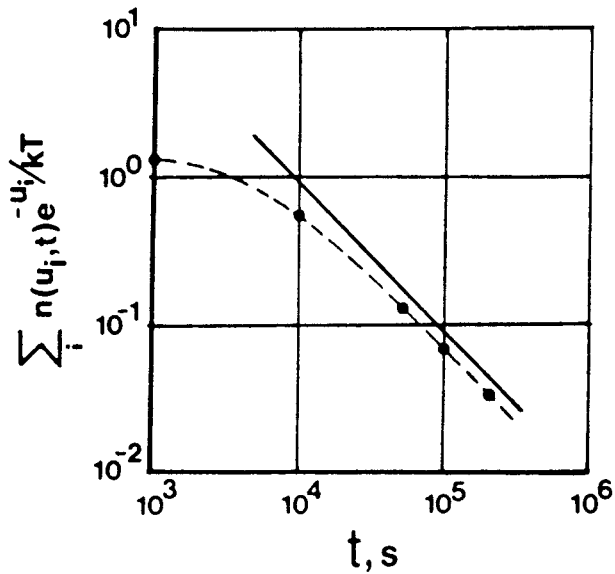Although the initial settlement rate appeared to be in perfect agreement with the log t creep law, the subsequent longer test periods at increased and normal temperatures showed deviations from this law (Fig 18). This can possibly be explained by the fact that the shear stresses in the model canister test were lower than about 20 % of the undrained shear strength of the clay, which was about 1 MPa. Thus, the softening effect caused by processes which lead to reduced barrier heights (par 5 in Chapter 5.2.1) may have been insignificant. This case has also been investigated by using the same basic stochastic theory that was applied in the preceding chapter, which then naturally yields a faster retardation of the strain (14). For the particular case of no softening effect at all, the theoretical shear strain is of the form:

$$\gamma = \alpha t - \beta t^2 + \gamma \qquad (t \leq \frac{\alpha}{2\beta} \text{ for } \gamma = c) \tag{20}$$

i.e. it starts off linearly and then dies out. We see from Fig 25 that curve fitting actually yields a curve shape that fits the entire range of observations up to 115 days relatively well, which supports the idea that the experimentally observed retardation beyond logarithmic decay is at least partly due to the low stress level. Expressing time in days the settlement in microns fit the following equivalent of Eq. (20):

$$s = 0.188t - 0.000813t^2 + 8.12 \tag{21}$$

It cannot be excluded, however, that there are other contributions to the deviation from the log t law. One is offered by considering heat-induced microstructural changes (5). Thus, a probable effect of heating is a contraction and expulsion of interlamellar hydrates associated with an increase in the amount of free water in adjacent pores with concomitant reduction in microstructural rigidity. At cooling, there would logically be a transfer of interaggregate water back to interlamellar positions leading to an increased resistance to shear that is possibly manifested by the observed deviation from the log t law. This transfer and arrival at equilibrium of the interlamellar water is known to take many weeks or even months as indicated by NMR determination of proton relaxation following mechanical dis-

turbance (15, 16, which would be in agreement with the slow change in shape of the settlement curve. Another possible heat effect could be an improved structural order of interlamellar hydrates by thermally aided disappearance of vacancies or defects leading to a more stable state of the structural units ("hardening"). Finally, heating to 70°C may have caused slight dissolution of silica and precipitation of amorphous hydrous silica compounds in the subsequent cooling period. The resulting strengthening effect is expected to be important at significantly higher temperatures but may have had some very slight effect also in the present test (5).
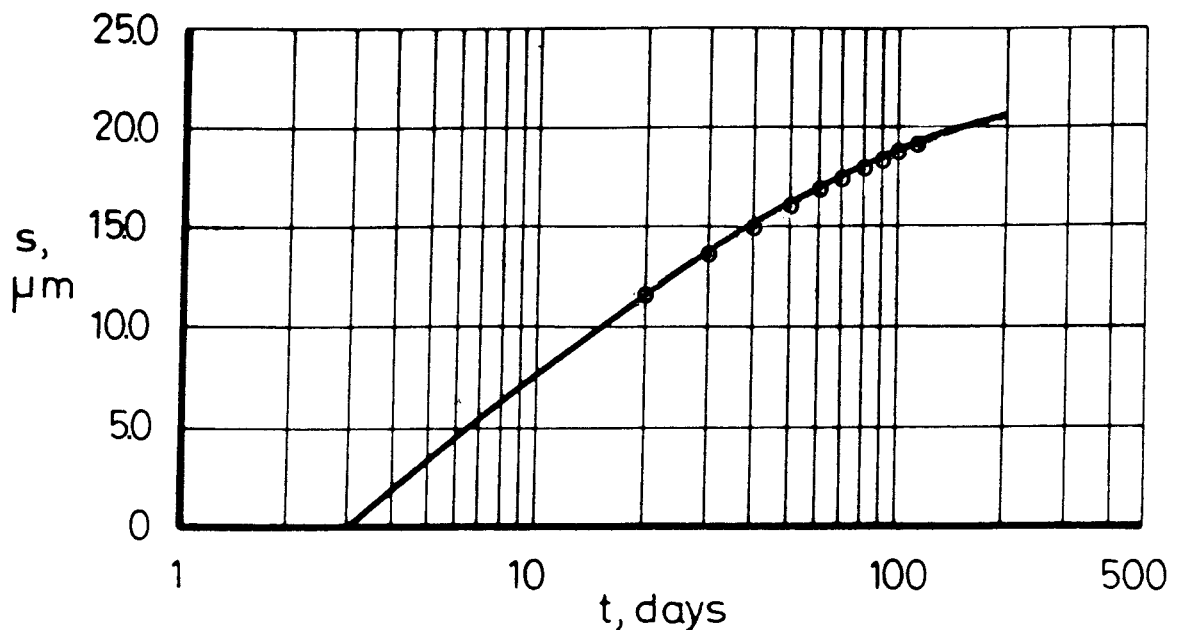

Fig 25. Curve fitting of Eq. (20) to the observed settlement (cf. Fig 18) during the second heating period. The rings refer to Eq. (21)

5.2.3   Physical nature of the energy barriers

The creep model implies that there is a spread in activation energy over a large range in the initial state, while the spectrum becomes more narrow and leads to a dominance of higher barriers in the course of the creep. Initially, the spectrum encompasses the range of the hydrogen bond and this is still the case at very high t-values but the majority of the barriers then appear to represent higher activation energies suggesting that electrostatic bonds and mass forces ultimately become predominant. It is not known at present whether the character of stochastic creep is retained over very long periods of time since the physical state of the interlamellar water is not sufficiently understood. Thus, it may well be that the degree of molecular order is enhanced by the creep, possibly in conjunction with thermal treatment, by which a more genuine plastic behavior of the montmorillonite "pseudocrystal" stacks may be produced. This would in turn strengthen the system and retard the settlement significantly.

6   RECOMMENDATIONS

Although the main mechanisms which yield canister settlement have been identified and the rate can be predicted with reasonable accuracy over long periods of time, the detailed understanding of the creep processes on a molecular scale is still not complete. For this purpose the question concerning the crystal constitution of montmorillonite needs to be clarified, a possible method of potential use being NMR technique combined with electron diffraction analyses.

Since the experimental study was made on a small geometrical scale it is strongly recommended to conduct a similar test with a larger canister, preferably in rock. Such a study should also comprise temperature cycling with the objective to determine the thermo-mechanical parameters, which could only be qualitatively investigated in the laboratory test. Such a study is presently prepared in the Stripa mine.

Finally, it appears that a more detailed study of the consolidation and flow mechanisms require finite element calculation of the strain yielding settlement. By this, the properties of individual clay elements can be varied independently which is not possible by using boundary element technique of the presently applied type. Suitable programs should be developed for this purpose.

7   ACKNOWLEDGEMENTS

8   REFERENCES

1   Pusch, R., Börgesson, L., & Ramqvist, G. Final Report of the
     Borehole, Shaft and Tunnel Sealing Test - Volume III:
     Tunnel Plugging. Stripa Project (In press)

2   Forslind, E., & Jacobsson, A. Water, a Comprehensive Treatise
     (Ed. Franks). Vol. 5, Ch 4, Clay-water systems, Plenum,
     New York, 1972 (pp 173-248)

3   Pusch, R. Chemical Interaction of Clay Buffer Materials and
     Concrete. Arbetsrapport SFR 82-01, SKBF/KBS, Nov 1982

4   Pusch, R., & Karnland, 0. Aspects of the Physical State of
     Adsorbed Water. SKB Technical Report, 1986 (In press)

5   Pusch, R. Permanent Crystal Lattice Contraction - A Primary
     Mechanism in Thermally Induced Alteration of Na-Bentonite.
     Proc. MRS 1986 Fall Meeting, Boston, USA 1986 (In press)

6   Sposito, G. The Surface Chemistry of Soils. Oxford Univ Press
     N.Y. & Clarendon Press Oxford, 1984 (p 67)

7   Pusch, R. A Technique for Investigation of Clay Microstructure.
     J. Microscopic, Vol. 6, 1967 (pp 963-986)

8   Housel, W.S.: Applied Soil Mechanics, Edw. Broth. Inc., Mich.,
     1960

9   Dawson, P.R., Chavez, P.F., Lipkin, J., & Silva, A.J.: Creep of
     Ocean Sediments Resulting from the Isolation of Radio-
     active Wastes. 2nd Ocean Dumping Conf., (Int. Rep), 1980

10   Pusch, R., & Feltham, P. A Stochastic Model of the Creep of
     Soils. Geotechnique Vol. 30, No. 4, 1980 (pp 497-506)

11   Pusch, R., Adey, R. Settlement of Clay-enveloped Radioactive
     Canisters. Appl. Clay Science, Vol. 1, 1986 (pp 353-365)

12   Börgesson, L. Water Flow and Swelling Pressure in Non-saturated
        Bentonite-based Clay Barriers. Eng. Geology, Vol. 21, No.
        3/4, 1985 (pp. 229-237)

13   Pusch, R. & Feltham, P. Computer Simulation of Creep of Clay.
        Proc. ASCE, J. Geot. Eng. Div., Vol. 107, No GT 1, 1981
        (pp. 95-104)

14   Pusch, R. A Physical Clay Creep Model and its Mathematical
        Analogy. Third Int. Conf. Numer Methods in Geomechanics,
        Aachen, 2-6 April 1979 (pp 485-492)

15   Jacobsson, A., & Pusch, R. Thixotropic Action in Remoulded Quick
        Clay. Bull. Int. Ass. Eng. Geology, No. 5, 1972 (pp 105-
        110)

16   Carlsson, T. Interactions in MX-80 Bentonite/water/electrolyte
        Systems. D. Thesis 1986:55 D, University of Luleå, 1986 (p
        71)

List of SKB reports

Annual Reports

1977-78
TR 121
KBS Technical Reports 1 – 120.
Summaries. Stockholm, May 1979.

1979
TR 79–28
The KBS Annual Report 1979.
KBS Technical Reports 79-01 – 79-27.
Summaries. Stockholm, March 1980.

1980
TR 80–26
The KBS Annual Report 1980.
KBS Technical Reports 80-01 – 80-25.
Summaries. Stockholm, March 1981.

1981
TR 81–17
The KBS Annual Report 1981.
KBS Technical Reports 81-01 – 81-16.
Summaries. Stockholm, April 1982.

1982
TR 82–28
The KBS Annual Report 1982.
KBS Technical Reports 82-01 – 82-27.
Summaries. Stockholm, July 1983.

1983
TR 83–77
The KBS Annual Report 1983.
KBS Technical Reports 83-01 – 83-76
Summaries. Stockholm, June 1984.

1984

TR 85–01
Annual Research and Development Report 1984
Including Summaries of Technical Reports Issued during 1984. (Technical Reports 84-01– 84-19)
Stockholm June 1985.

1985
TR 85-20
Annual Research and Development Report 1985
Including Summaries of Technical Reports Issued during 1985. (Technical Reports 85-01-85-19)
Stockholm May 1986.

Technical Reports

1986

TR 86-01
I: An analogue validation study of natural radionuclide migration in crystalline rock using uranium-series disequilibrium studies
II: A comparison of neutron activation and alpha spectroscopy analyses of thorium in crystalline rocks
J A T Smellie, Swedish Geological Co, A B MacKenzie and R D Scott, Scottish Universities Research Reactor Centre
February 1986

TR 86-02
Formation and transport of americium pseudocolloids in aqueous systems
U Olofsson
Chalmers University of Technology, Gothenburg, Sweden
B Allard
University of Linköping, Sweden
March 26, 1986

TR 86-03
Redox chemistry of deep groundwaters in Sweden
D Kirk Nordstrom
US Geological Survey, Menlo Park, USA
Ignasi Puigdomenech
Royal Institute of Technology, Stockholm, Sweden
April 1, 1986

TR 86-04
Hydrogen production in alpha-irradiated bentonite
Trygve Eriksen
Royal Institute of Technology, Stockholm, Sweden
Hilbert Christensen
Studsvik Energiteknik AB, Nyköping, Sweden
Erling Bjergbakke
Risö National Laboratory, Roskilde, Denmark
March 1986

TR 86-05
Preliminary investigations of fracture zones in the Brändan area, Finnsjön study site
Kaj Ahlbom, Peter Andersson, Lennart Ekman, Erik Gustafsson, John Smellie,
Swedish Geological Co, Uppsala
Eva-Lena Tullborg, Swedish Geological Co, Göteborg
February 1986

TR 86-06
Geological and tectonic description of the Klipperås study site
Andrzej Olkiewicz
Vladislav Stejskal
Swedish Geological Company
Uppsala, October, 1986

TR 86-07
Geophysical investigations at the Klipperås study site
Stefan Sehlstedt
Leif Stenberg
Swedish Geological Company
Luleå, July 1986

TR 86-08
Hydrogeological investigations at the Klipperås study site
Bengt Gentzschein
Swedish Geological Company
Uppsala, June 1986

TR 86-09
Geophysical laboratory investigations on core samples from the Klipperås study site
Leif Stenberg
Swedish Geological Company
Luleå, July 1986

TR 86-10
Fissure fillings from the Klipperås study site
Eva-Lena Tullborg
Swedish Geological Company
Göteborg, June 1986

TR 86-11
Hydraulic fracturing rock stress measurements in borehole Gi-1, Gideå Study Site, Sweden
Bjarni Bjarnason and Ove Stephansson
Division of Rock Mechanics,
Luleå University of Technology, Sweden
April 1986

TR 86-12
PLAN 86— Costs for management of the radioactive waste from nuclear power production
Swedish Nuclear Fuel and Waste Management Co
June 1986

TR 86-13
Radionuclide transport in fast channels in crystalline rock
Anders Rasmuson, Ivars Neretnieks
Department of Chemical Engineering
Royal Institute of Technology, Stockholm
March 1985

TR 86-14
Migration of fission products and actinides in compacted bentonite
Börje Torstenfelt
Department of Neclear Chemistry, Chalmers
University of Technology, Göteborg
Bert Allard
Department of water in environment and society, Linköping university, Linköping
April 24, 1986

TR 86-15
Biosphere data base revision
Ulla Bergström, Karin Andersson, Björn Sundblad, Studsvik Energiteknik AB, Nyköping
December 1985

TR 86-16
Site investigation
Equipment for geological, geophysical, hydrogeological and hydrochemical characterization
Karl-Erik Almén, SKB, Stockholm
Olle Andersson, IPA-Konsult AB, Oskarshamn
Bengt Fridh, Bengt-Erik Johansson,
Mikael Sehlstedt, Swedish Geological Co, Malå
Erik Gustafsson, Kenth Hansson, Olle Olsson,
Swedish Geological Co, Uppsala
Göran Nilsson, Swedish Geological Co, Luleå
Karin Axelsen, Peter Wikberg, Royal Institute of Technology, Stocholm
November 1986

TR 86-17
Analysis of groundwater from deep boreholes in Klipperås
Sif Laurent
IVL, Swedish Environmental Research Institute
Stockholm, 1986-09-22

TR 86-18
Technology and costs for decommissioning the Swedish nuclear power plants.
Swedish Nuclear Fuel and Waste Management Co
May 1986

TR 86-19
Correlation between tectonic lineaments and permeability values of crystalline bedrock in the Gideå area
Lars O Ericsson, Bo Ronge
VIAK AB, Vällingby
November 1986

TR 86-20
A Preliminary Structural Analysis of the Pattern of Post-Glacial Faults in Northern Sweden
Christopher Talbot, Uppsala University
October 1986

TR 86-21
Steady-State Flow in a Rock Mass Inte sected by Permeable Fracture Zones. Calculations on Case 2 with the GWHRT-code within Level 1 of the HYDROCOIN Project.
Björn Lindbom, KEMAKTA Consultants Co, Stockholm
December 1986

TR 86-22
Description of Hydrogeological Data in SKBs Database Geotab
Bengt Gentzschein, Swedish Geological Co, Uppsala
December 1986